Palaeogeography, Palaeoclimatology, Palaeoecology 443 (2016) 80–97

Contents lists available at ScienceDirect

Palaeogeography, Palaeoclimatology, Palaeoecology

journal homepage: www.elsevier.com/locate/palaeo

Late Jurassic biogeochemical microenvironments associated with microbialite-coated unionids (Bivalvia), Asturias (N Spain)

R.P. Lozano [a], G. Delvene [a], L. Piñuela [b], J.C. García-Ramos [b]

[a] Museo Geominero, Instituto Geológico y Minero de España (IGME), C/Ríos Rosas 23, 28003 Madrid, Spain
[b] Museo del Jurásico de Asturias, 33328 Colunga, Spain

ARTICLE INFO

Article history:
Received 23 September 2015
Received in revised form 19 November 2015
Accepted 20 November 2015
Available online 2 December 2015

Keywords:
Freshwater
Oncoid
Bivalve
Hot springs
Wetland
Kimmeridgian

ABSTRACT

The Vega Formation (Upper Jurassic, Asturias, Spain) contains two Kimmeridgian outcrops – the Abeu and Huerres sections – with bivalves coated with carbonate microbialites (oncoids). The bivalve shells in the Abeu section were replaced early by calcite, while those of the Huerres section were dissolved and the moulds filled by late diagenetic cements. For the Abeu shells, there was a loss of Sr and a gain of Mg, Fe and Mn during the replacement process, but much of the original organic matter was retained. Part of the S present can be linked to this organic matter, and part to the sulphate that replaced the carbonate groups in the calcite. The thin microbialites inside the shells of some of the Huerres bivalves have allowed us to estimate the influence of the growth rate on the incorporation of trace elements in calcite. With an approximately six times lower growth rate, the internal microbialite incorporates less Mg and S and more Fe and Mn than the external one, while maintaining the Sr content. The trace element content (Mg, S, Sr, Fe and Mn) of the Huerres and Abeu microbialites are similar; these coatings may therefore have been formed in the same type of freshwater but in different microenvironments. Given the substantial sulphate content of the microbialites from both sections, this freshwater probably came from hot springs. However, the high Fe/Mn ratio of the Abeu microbialites suggests a reducing environment during their formation. Indeed, $\delta^{18}O$ and $\delta^{13}C$ data confirm that the Abeu and Huerres microbialites were formed in different microenvironments: the positive covariance for $\delta^{18}O$ and $\delta^{13}C$ of the Abeu microbialites and replaced shells ($r^2 = 0.83$) and the wide range of variation for $\delta^{18}O$ (2.80‰) together suggest that the microbialite crusts grew in isolated ponds where evaporation was dominant. In the Huerres microbialites the positive covariance for $\delta^{18}O$ and $\delta^{13}C$ ($r^2 = 0.59$) and the narrow range of variation for $\delta^{18}O$ (0.74‰) indicate that the Huerres section was formed in a more open environmental system where degassing predominated over evaporation.

1. Introduction

Oncoids – a term coined by Heim (1916) for the micritic grains found in Jurassic shelf limestones in Switzerland – are a variety of microbialite. These spherical or pseudo-spherical biosedimentary structures form as successive laminations around both biogenic and non-biogenic nuclei (Zaton et al., 2012). Most oncoids are found in carbonate rocks where the biological precipitation of carbonate was promoted by photosynthetic microbes (predominantly cyanobacteria) (Weiner and Dove, 2003). Since they must photosynthesise, cyanobacteria grow in shallow water (Mur et al., 1999). The CO_2 they consume increases the pH of their environment, inducing the precipitation of calcium carbonate, normally as calcite (Dupraz et al., 2008).

Microbialites from Jurassic fluvial and lacustrine environments are poorly known (Neuhauser et al., 1987; Perry, 1994; Dunagan and Turner, 2004; Whiteside, 2005; Bosence, 2012; Arenas et al., 2015), although shell-core oncoids are relatively well represented in the fossil record (Galiana, 1979; Lindqvist, 1994; Gradzinski et al., 2004; Qvarnström, 2012). Oncoid deposits are a relatively common feature of many non-marine carbonate facies, but there are fewer references to oncoids forming around freshwater unionid shells. These latter include Oligocene lacustrine oncoids in Germany (Leinfelder and Hartkopf-Fröder, 1990), Miocene bivalves in lake deposits in New Zealand (Lindqvist, 1994), Mesozoic bivalves of the Upper Jurassic–Lower Cretaceous in northern Spain (Hernández Gómez, 2000), Upper Triassic oncoids in southern Poland (Szulc et al., 2006) and oncoidal facies of the Upper Cretaceous–Palaeocene in Spain (Astibia et al., 2012).

Studies on recent aragonite shells from continental environments demonstrate the usefulness of geochemical studies on shells for palaeoenvironmental reconstructions (Yan et al., 2014, among others). The main problem is that the original aragonite in fossil shells is typically replaced by calcite or is dissolved during diagenesis (Wright and Cherns, 2009; Bayer et al., 2013), and only in very exceptional cases is any relict aragonite preserved (Carter and Tevesz, 1978; Sandberg and Hudson, 1983; Brand, 1989; Pirrie and Marshall, 1990; Purton et al.,

E-mail addresses: r.lozano@igme.es (R.P. Lozano), g.delvene@igme.es (G. Delvene), lpinuela.muja@gmail.com (L. Piñuela).

http://dx.doi.org/10.1016/j.palaeo.2015.11.021
0031-0182/

1999; Hendry et al., 2001). Consequently, many researchers have ruled out the geochemical study of shells because the replacement process modifies their original chemistry. Therefore, very little literature exists on the study of replaced ancient shells to reconstruct palaeoecosystems, although some marine examples have been published by Ivany and Runnegar (2010). The literature on continental replaced shells as a tool for palaeoecological reconstructions is even scarcer. The present study, however, demonstrates that the calcite which replaced the original aragonite of Spanish Jurassic freshwater bivalves contains useful palaeoenvironmental information. Although such bivalves are uncommon and generally poorly known, recent studies on the Upper Jurassic rocks of several localities in the northern and eastern Iberian Peninsula have yielded interesting information regarding the occurrence of these molluscs in several freshwater environments (Delvene et al., 2013a).

In marine and freshwater environments, precipitation of the trace elements in calcite is determined by Mg/Ca, Sr/Ca, Fe/Ca and Mn/Ca ratios, redox conditions, salinity, P_{CO2} and the temperature of the solution (Barnaby and Rimstidt, 1989; Ihlenfeld et al., 2003). However, other factors, such as the calcite growth rate, determine the incorporation of trace elements and directly affect the partition coefficients (Mucci, 1988; Huang and Fairchild, 2001). Partition coefficients are applicable in a wide variety of geological studies, such as the conditions of precipitation of marine (e.g. Burton and Walter, 1991; Gray et al., 2014) and continental calcite (e.g; Ihlenfeld et al., 2003; Carroll and Romanek, 2008), and modelling of meteoric and burial processes of carbonate diagenesis (e.g. Banner, 1995; Pavlovic et al., 2002). In some of the bivalves studied here, two microbialites that differed in growth rate and trace element content were developed at the same time in water presenting similar geochemical properties: a thick external layer (external microbialite) and a thin inner cover (internal microbialite). These new data can be applied in calcite of different origin and are particularly important to consider in future palaeoenvironmental freshwater carbonate interpretations, especially in palaeoclimatic studies of calcite speleothems (Huang and Fairchild, 2001; Rossi et al., 2014).

The oncoid formations are associated with springs based on: a) textural characteristics and b) existence of synsedimentary faults at nearby outcrops (García-Ramos et al., 2010b). In the present paper we demonstrate the influence of hot springs on microbialite formation based on geochemical evidence (S content). Sulphate is usually preserved in a lattice-bound form, indicating the substitution in sedimentary calcite of tetrahedral SO_4 by planar CO_3 ions (Kontrec et al., 2004). Continental sedimentary carbonates only incorporate small amounts of S (Staudt and Schoonen, 1995), unless they were formed in hot springs where the S content can be much higher (Takano et al., 1980; Fouke et al., 2000). Chemical, isotopic and textural studies were conducted on the shells and their oncoids. In addition, the processes of replacement of the bivalve shell and the formation of post-burial diagenetic carbonates were analysed. The aim of the present study was to characterise the nature of continental microenvironments in the marginal wetland fault-related settings of the Vega Formation (a fluvial formation in Asturias) by analysing the geochemistry (TOC, trace and stable isotope elements) of in-place microbial carbonates that recorded the water chemistry prevalent at that time (Upper Jurassic).

2. Geological setting

The best-preserved Jurassic outcrops in Asturias (northern Spain) are about 60 km long on the coast between Cabo Torres in Gijón and the Arra beach in Ribadesella (García-Ramos et al., 2011; Fig. 1). The Jurassic succession, in which these outcrops are found, lies in the Gijón-Villaviciosa Basin (Ramírez del Pozo, 1969), which itself is bound to the west and east by the Veriña and Ribadesella faults, respectively (Lepvrier and Martínez García, 1990; Alonso et al., 2009). The Jurassic succession of Asturias (Fig. 2) has been grouped into two high-order lithological units (Valenzuela et al., 1986; Meléndez et al., 2002). The lower one (the Villaviciosa Group) is predominantly composed of carbonate rocks of littoral and shallow marine origin (Gijón and Rodiles formations), while the upper one (the Ribadesella Group) mainly contains terrestrial siliciclastic rocks of alluvial fan and fluvial origin (the La Ñora and Vega formations, respectively), together with restricted shallow sea deposits (a shelf lagoon) of the Tereñes Formation, and fluvial-dominated lagoonal delta deposits (the Lastres Formation).

The Upper Jurassic Vega Formation (160 m thick) comprises a laterally variable succession dominated by white and reddish sandstones, red mudstones with some siliceous and calcareous conglomeratic

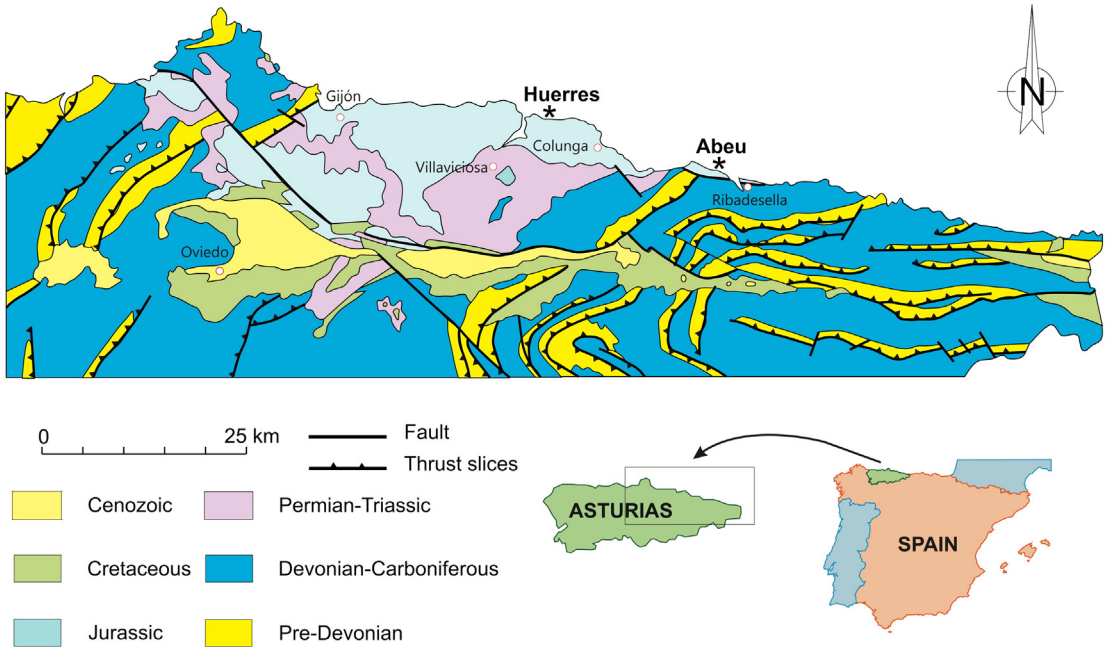

Fig. 1. Location of Huerres and Abeu sections in Colunga and Ribadesella, respectively (Asturias, N Spain). Geological map of the central-eastern area of Asturias based on the cartography of the Geology Department, University of Oviedo (modified after García-Ramos and Gutiérrez Claverol, 1995).

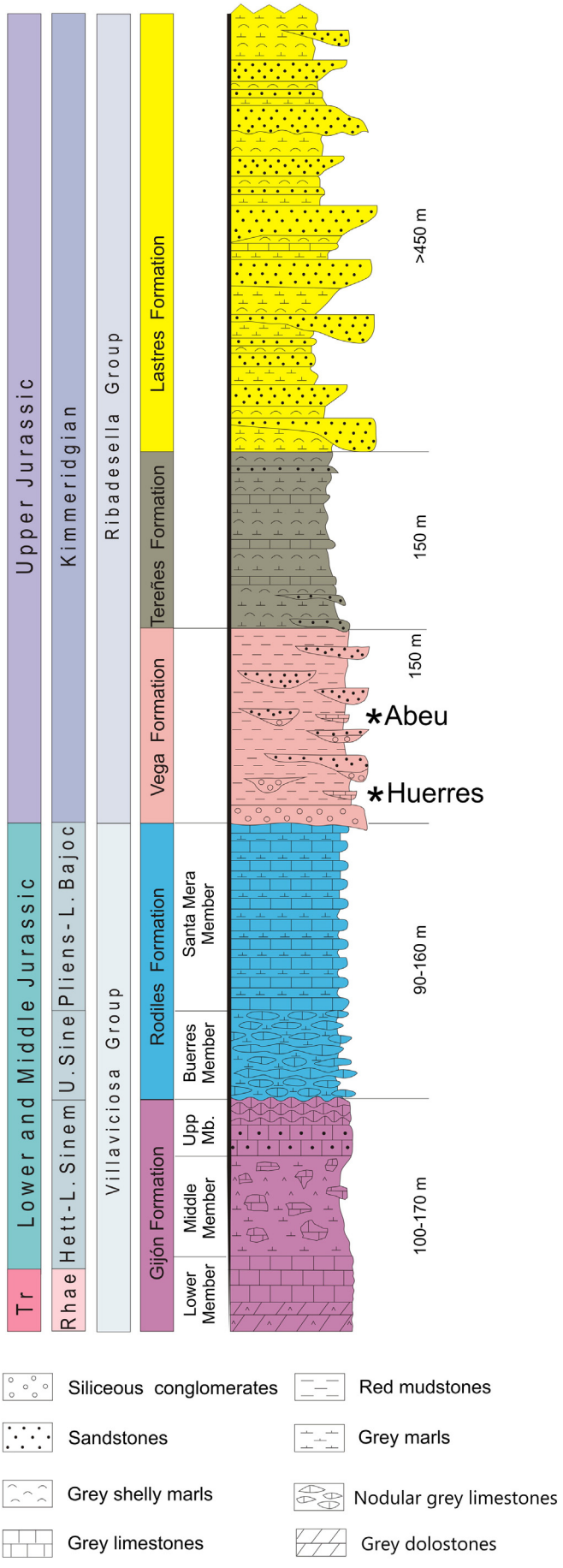

intercalations, and minor grey limestones and marls (García-Ramos et al., 2010a). This sequence constitutes a series of metre-scale fining-upwards cycles deposited on an alluvial plain (axial fluvial system). This was crossed by ephemeral or intermittent, high sinuosity rivers under predominantly semi-arid climatic conditions, favouring the development of frequent and extensive calcrete palaeosols on the floodplains (García-Ramos et al., 2010a; Gutierrez and Sheldon, 2012), as well as sporadic ponds and small depressions with high microbial activity (stromatolites and oncoids). These wetlands were the foci for the deposition of grey limestones and marls with frequent oncoid concentrations. Their fluvial–lacustrine and palustrine carbonate systems were fed by a number of carbonate-rich freshwater springs originating from major normal faults. The waters came from neighbouring uplifted and palaeo-karstified limestones and dolostones in the south consisting of the uppermost Triassic–Lower Jurassic rocks of the Gijón and Rodiles formations (García-Ramos et al., 2010a, 2010b; Arenas et al., 2015).

The polygenic calcareous conglomerates, which are often interbedded with a limestone–marl facies association, represent the distal areas of small, marginal alluvial fan systems derived from nearby uppermost Triassic–Lower Jurassic calcareous palaeoreliefs. Located at the south, these were controlled by major synsedimentary faults subject to tectonic reactivation. The activity of these synsedimentary normal faults produced rapid variations in both the thickness and the facies of the Vega Formation. This included a relative increase in the proportion of coarse carbonate clasts compared to the main axial siliciclastic fluvial system, especially in marginal areas close to fault-controlled calcareous reliefs.

Extensional tectonics (rifting) in this area during the Late Jurassic–Early Cretaceous was linked to an initial phase in the opening of the Bay of Biscay and the Central Atlantic (Hiscott et al., 1990; Ziegler, 1990; Robles et al., 2002; Aurell et al., 2003; Uzqueda et al., 2013). Based on its ostracods (Schudack, 1987; Schudack and Schudack, 2002), the Vega Formation probably dates from the Late Oxfordian to Late Kimmeridgian. However, its pollen and spores suggest a post-Oxfordian age (Barrón, 2010). The unit rests on a significant regional unconformity, which erosively truncates a thick succession of marine Jurassic carbonates (Rodiles Formation, Fig. 1). This emersion, which resulted in a sudden shift from marine to terrestrial conditions, is made spectacularly clear by the sharp contact between the siliciclastic rocks of the Vega Formation and their underlying carbonates. The unconformity can nowadays be observed in several outcrops in the east-central sector of the coastal cliffs (Fig. 1).

2.1. The studied sections

The studied Abeu and Huerres sections are located in two coastal outcrops of the Vega Formation, and contain carbonate beds with freshwater bivalves (unionids) serving as oncoid nuclei (Figs. 1, 2).

2.1.1. The Abeu section

The main bed containing microbialite-coated freshwater bivalves is a 1.2-m-thick grey limestone layer with several calcareous marl intercalations (upper unit) (Fig. 3A). The molluscs occur concentrated in multiple lenticular scoured limestones (bivalve-intraclast rudstones and packstones), which pass upwards into calcareous marls with wackestone to mudstone textures. Both lithologies are arranged in cm-sized graded beds to dm-scale fining-upwards cycles. Small oncoids are present (though rare), together with charophyte debris and some flattened logs up to 40 cm in length.

This bed erosively overlies a 1.5-m-thick grey marl bed (middle unit) characterised by deformation structures (convolute bedding and slumps) which are more common in the upper part. Other minor

Fig. 2. General log (not to scale) of the Asturian Jurassic (modified after García-Ramos et al., 2011).

Fig. 3. A: Field view of the Abeu outcrop, aspect of the erosional surface between the middle (MU) and the upper (UU) units. Note the rapid wedging out of the (UU) to the right; lower unit (LU). B–E. Field views of different aspects of the Huerres outcrop. B: Oncoid in situ, reflecting the shape of the bivalve nuclei. C/D: Sections of elongated oncoidal coatings on vanished phytoclasts replaced by calcite. E: Natural cross-section of oncoid whose nucleus is a bivalve. Note the external micropustular aspect (arrow), and the white calcite of the replaced shell.

components include a number of irregular stromatolitic fragments, charophyte debris and rare tubular oncoids with nuclei replaced by sparry calcite. The base of this middle unit represents a high-relief erosional surface (palaeo-channel) controlled, at least on one of its margins, by a small synsedimentary fault. The unit rapidly wedges out laterally and is replaced by reddish mudstones with calcrete palaeosols.

The lower unit is similar in composition and structure to the upper unit but contains some micro-oncoids, ooids, pellets and small fragments of black limestone, but no freshwater bivalves. These grey limestone–marl deposits are intercalated between a predominantly reddish siliciclastic succession of fluvial origin, and reflect a freshwater carbonate wetland–pond system located in topographic lows controlled by small synsedimentary faults. The predominant grey coloration of the sediments (indicating their formation in a reducing environment) suggests a permanently saturated gleyed area with a relatively high water table. The high-relief channelised base of the middle carbonate unit and its rapid lateral transition upstream to reddish fine-grained beds with calcretes may represent a relatively high-gradient gully excavated by spring-fed water currents. Convolute and slump structures are probably related to sliding processes on the abrupt slope margins of the gully.

The carbonate upper unit with freshwater bivalves represents the last stages of the infill of the gully on the pond margin prior to the final deactivation of the carbonate wetland system due to a new reactivation of siliciclastic fluvial supplies. Similar wetland systems in semiarid regions have been reported in many studies (Sandford, 1995; Dunagan and Turner, 2004; Djamali et al., 2006; Dunagan, 2007; Tooth and McCarthy, 2007; Jennings et al., 2011; Cabaleri et al., 2013).

2.1.2. The Huerres section

The Huerres section is a small and discontinuous outcrop associated with a minor (secondary) E–W trending synsedimentary fault (García-Ramos et al., 2010b; Uzkeda et al., 2013). It is equivalent to the La Griega section described by Arenas et al. (2015). The outcrop shows a

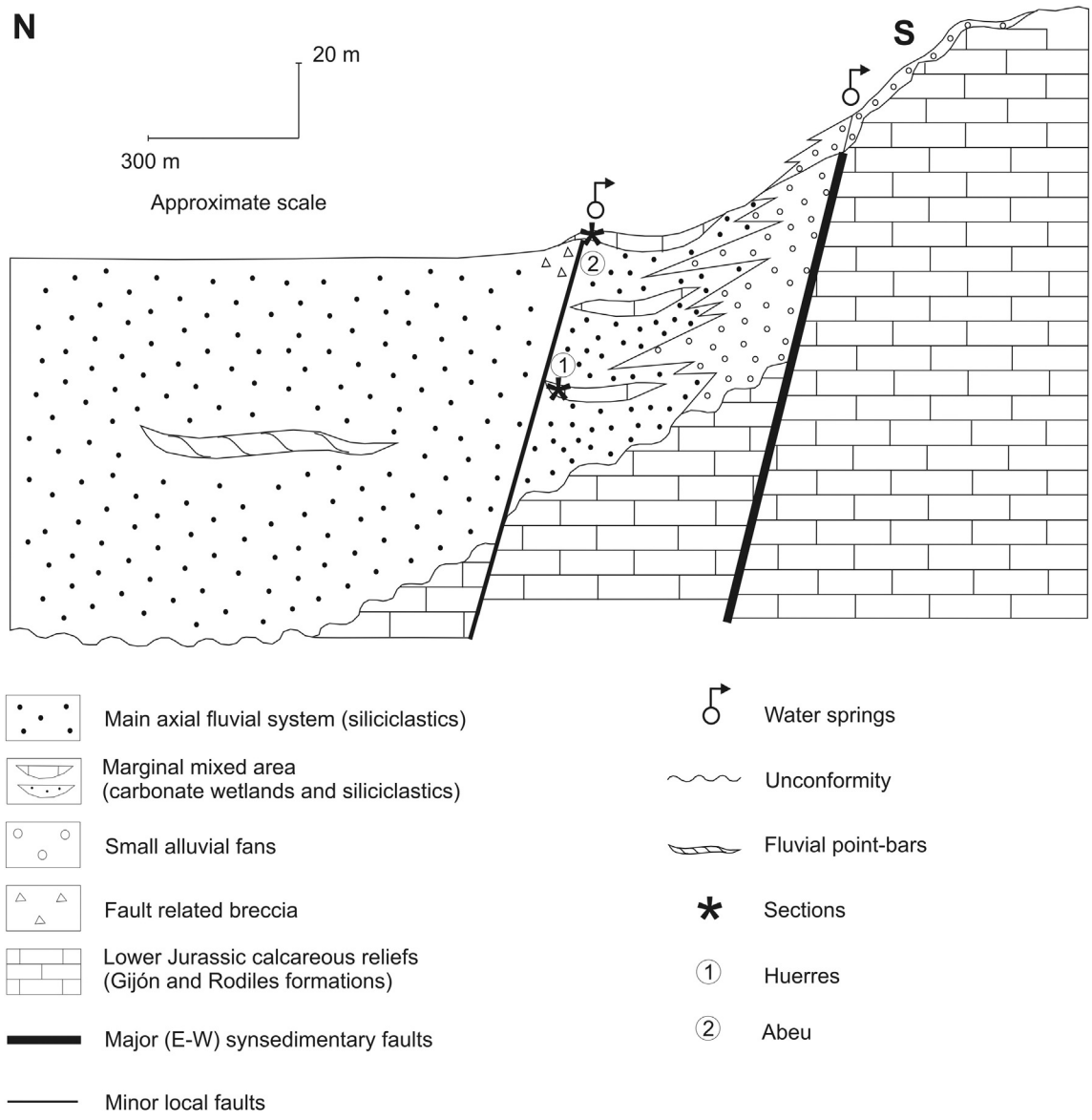

Fig. 4. Idealized (composite) cross-section roughly perpendicular to the southern faulted margin of the basin during deposition of the Vega Formation sedimentary succession.

channelised polygenic calcareous microconglomerate erosively overlain by an oncoid–intraclast rudstone dominated by freshwater bivalve shells with microbial coatings, passing upwards to intraclast packstone and wackestone (Fig. 4; see Arenas et al., 2015, for more details). The oncoid–intraclast rudstone occasionally includes some phytoclasts with sparry calcite nuclei and stromatolite fragments (Fig. 3C–D). The main oncoidal bed (oncolite) of the La Griega section is dominated by pebble- to cobble-sized oncoids that are nearly spherical, oval, irregular or cylindrical in shape.

The polygenic calcareous microconglomerate includes mainly carbonate clasts from underlying marine Jurassic units (Gijón and Rodiles formations), together with intraformational limestone and lutitic fragments from the Vega Formation. Their origin is related to the channelised flows of middle to distal areas of small alluvial fans of southern provenance, created by the reactivation of E–W trending old basement (Late Variscan) faults (García-Ramos et al., 2010b; Arenas et al., 2015). In the Asturian Basin, the Llanera and Ribadesella faults are similar reactivated structures of identical orientation and significance (Alonso et al., 2009).

The pebble- and cobble-sized channelised oncoids (including those with unionid nuclei, Fig. 3B) overlying the calcareous microconglomerates probably represent reworked clasts from small ponds that developed in local fault-controlled depressions housing wetlands and which produced siliciclastic sediment-starved areas lateral to the main axial fluvial system. The poor sorting of the oncoids, the fining-upwards trend, and the channelised base of the bed suggest that the latter was produced by extreme flooding events associated with heavy rainfall periods.

Fig. 5. Macro- and microscopic features of bivalves. A: Unionida. Right valve. MUJA-4281. Note the micropustular crust on the shell. Vega Fm, Abeu section (Ribadesella, Asturias). B–C: Unionida MUJA-4275. B: Right, C: left views of an articulated specimen without microbialitic crust. Vega Fm, Abeu section (Ribadesella, Asturias). D–E: Unionida. Note the micropustular aspect of the crust in both valves of an articulated specimen. Vega Fm, Abeu section (Ribadesella, Asturias). F–G: Large oncoid with a unionoid bivalve as nucleus. F: External aspect of the microbialitic crust. G: Lateral view showing the crust and the internal mould of the bivalve. Vega Fm, Huerres section (La Griega beach, Colunga, Asturias). H: Optical microscopy view of thin-section showing the microstructure of a single valve of Unionida. Note the external prismatic layer, and the organic layers among the nacreous one. Vega Fm, Abeu section (Ribadesella, Asturias). I: Polished section of the previous specimen. Note lateral continuity of organic layers of the shell. Taxa cannot be named in this paper because they belong to a new taxa (Delvene et al., in press).

3. Methods

Forty oncoids with bivalve nuclei from a carbonate facies of the Abeu section, and 56 from a carbonate facies of the Huerres section (Fig. 1) were sectioned to examine their sedimentological, mineralogical and chemical features, together with their stable isotope compositions. Ninety-six sections were polished and their macrotextures examined using a conventional scanner. A binocular magnifier was then used to

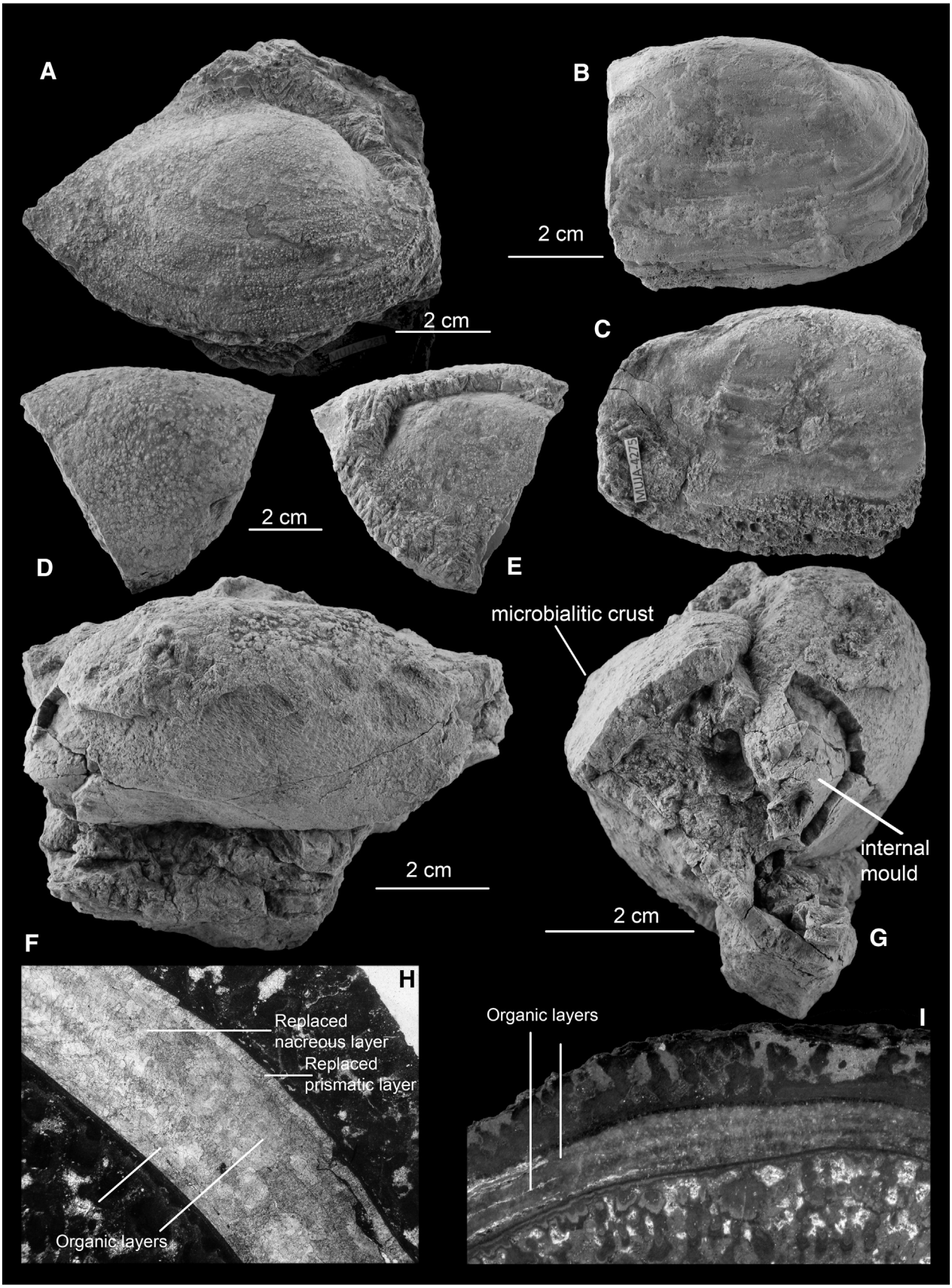

select points of analysis and areas where thin-sections would be cut. Fifteen polished thin-sections (7 Abeu and 8 Huerres) were made at the laboratories of the National Centre of Human Evolution, Burgos (Spain) and then examined using a petrographic microscope and an electron microprobe.

Selected samples of the oncoids were subjected to bulk powder X-ray diffraction (XRD) analysis using a Panalytical X'Pert PRO apparatus with a copper tube, a graphite monochromator and an automatic divergence slit (performed at the laboratories of the *Instituto Geológico y Minero de España*, IGME). Based on textural differences, several growth bands were subsampled and examined using a JEOL 6400 scanning electron microscope (SEM) equipped with an energy-dispersive X-ray (EDX) spectrometer.

Careful sampling for bulk content analyses was performed in areas of microbialite with no visible microspar cement — although the inclusion of some microspar was often inevitable. The bulk content results are therefore derived from a mix of microbialite and diagenetic calcite. A microprobe was used to establish the trace element content of the microbialites and microspar fillings of the primary porosity.

Six samples (4 Abeu and 2 Huerres samples) from areas where thin-sections showed minimal or no cement were selected for bulk analysis of trace elements and total organic carbon (TOC), and for stable isotope analysis. Extractions were performed with a microdrill. Sulphur and TOC were determined using an ELTRA-CS-800 IR analyzer. The samples were decalcified prior to TOC analyses by adding a few drops of HCl/$FeCl_2$ until all the calcium carbonate was removed and no further reaction was observed. The samples were then heated to 1800 °C and the TOC measured in terms of CO_2 by an infrared detector.

Bulk Ca and Mg content in four Abeu and two Huerres samples was analysed by atomic absorption spectroscopy (AAS) using a Varian SpectrAA 220 FS apparatus. Fe, Mn, Sr and Ba determinations were performed by inductively coupled plasma atomic emission spectroscopy (ICP-AES) using a Varian Vista-MPX spectrometer. The S, TOC and bulk Ca, Mg, Fe, Mn and Ba analyses were performed at the laboratories of the IGME (Spain).

Chemical analyses of replaced shell, microbialite and diagenetic cements were performed on graphite-coated polished thin-sections using a JEOL JXA 8900 electron probe microanalyser (EPMA) (15 kV, 20 nA, 10 μm beam diameter) (performed at the ICTS Spanish National Centre for Electron Microscopy, Complutense University of Madrid, Spain).

Thirty-seven samples (13 from Abeu and 24 from Huerres) were selected for bulk sample analyses of carbon and oxygen stable isotopes using a Finnigan MAT 251 triple-collector gas source mass spectrometer coupled to a Finnigan Kiel automated preparation device (performed at the Stable Isotope Laboratory of the University of Michigan, USA). The international standard NBS-19 ($\delta^{13}C$ V-PDB = +1.94‰ and $\delta^{18}O$ V-PDB = −2.19‰) was used. The results are reported in δ‰ notation relative to V-PDB. Overall reproducibility was better than ±0.04‰ for $\delta^{13}C$ and ±0.06‰ for $\delta^{18}O$.

4. Results

4.1. Macro- and microscopic features of the bivalves

Examination of the uppermost part of the Vega Formation (Kimmeridgian) – the Abeu section near the town of Ribadesella – revealed a number of articulated bivalve shells and single valves. These are the oldest fossil records of Unionida currently known from Spain (Delvene et al., 2013b). The bivalves are up to 68 mm in height and 100 mm in length, and most of them are covered with a compact calcite which is thicker on isolated valves (up to 9.4 mm thick) than on articulated valves (up to 2 mm thick; Fig. 5). The original composition of the shell was aragonite, which was replaced by brown calcite. This calcite obstructed both the preparation and the observation of some important external and internal features of the shells, rendering identification at species level difficulty.

The present specimens show the general microstructure of unionids: an external prismatic layer and a nacreous layer (although with no distinction between the inner and middle layers) (Fig. 5H, I). The prismatic layer is 300 μm thick and contains small (40–100 μm) elongated crystals arranged perpendicular to the shell surface. The nacreous layer is composed of an irregular mosaic of large euhedral crystals (150–500 μm), and contains visible organic layers.

The Huerres section (near La Griega beach) is characterised by an accumulation of oncoids, the nuclei of which are predominately formed by bivalves (Fig. 5F, G). These latter are either elongated or bulb-shaped with a microbialite cover showing different degrees of development. This cover represents a special kind of preservation that records the existence of specimens. The bivalves were up to 62 mm in height, >86 mm in length, thick-shelled (up to 5.2 mm), oval in outline, smooth, and ornamented only with commarginal growth lines. Delvene et al. (in press) consider them to represent a new taxon with intraspecific variability, ascribable to the Unionidae family.

4.2. Macro- and microscopic features of the microbialites

The present material shows two kinds of microbialite occurrence. In the Abeu section, partially microbialite-covered articulated specimens (incipient oncoids) were found (Fig. 6C), together with isolated valves completely covered by microbialite (well-developed oncoids) (Fig. 5D, E). In the Huerres section, all the oncoids are well developed, and mainly comprise articulated bivalves (Fig. 5F, G). Some isolated valves and plant remains also serve as nuclei.

4.2.1. The Abeu section record

The isolated valves are covered in microbialite up to 1 cm thick (Fig. 6A, B). Microbialite growth is asymmetric; more extensive growth can be seen either on the convex face of the shell (Leinfelder and Hartkopf-Fröder, 1990; Fig. 6A), or on the concave face (Fig. 6B). Under the petrographic and binocular microscopes, the coatings appear to display alternating dark and light laminations, with the dark one being in contact with the replaced shell (Fig. 7A). From the base of this replaced shell towards the top of the microbialite, the microstructure consists of (1) dark flat or slightly wavy layers around 500 μm thick, and (2) an interval of several domes, each approximately 1 mm thick. The upwards growth of the domes has resulted in the development of tiny cones, some of which are incipiently branched. The primary porosity of well-developed domes is mostly microsparite and partially replaced barite (Fig. 7A); occasionally, gypsum and scarce detritic elements (mainly quartz) are present. Pyrite (10–50 μm) appears dispersed among the oncolithic micrite and is also present in the matrix of the surrounding rock, although in a much larger form (maximum dimension 500 μm).

SEM images showed some cyanobacterial filament ghosts on the microbialite crusts, with spaces of 5 μm surrounded by micritic calcite crystals (2–10 μm), similar to those reported by Leinfelder and Hartkopf-Fröder (1990). The microbialite on the articulated bivalves is generally slightly distorted and fragmented (Fig. 6C), measuring only 100–200 μm thick (or absent), and flat or slightly undulating. Microbialite domes, however, are developed mainly on the umbo, with an alternation of light and dark laminations measuring between 1.5 and 2.5 mm thick (Figs. 6C, 7B). The valves show a micropustular exterior with small protuberances (0.4–0.8 mm in diameter) distributed homogeneously on the valve flanks (Figs. 3E, 5D-E).

Some isolated cyanobacterial filaments can be seen in the micritic matrix (Fig. 7C). Their small radial communities (3–4 mm in diameter)

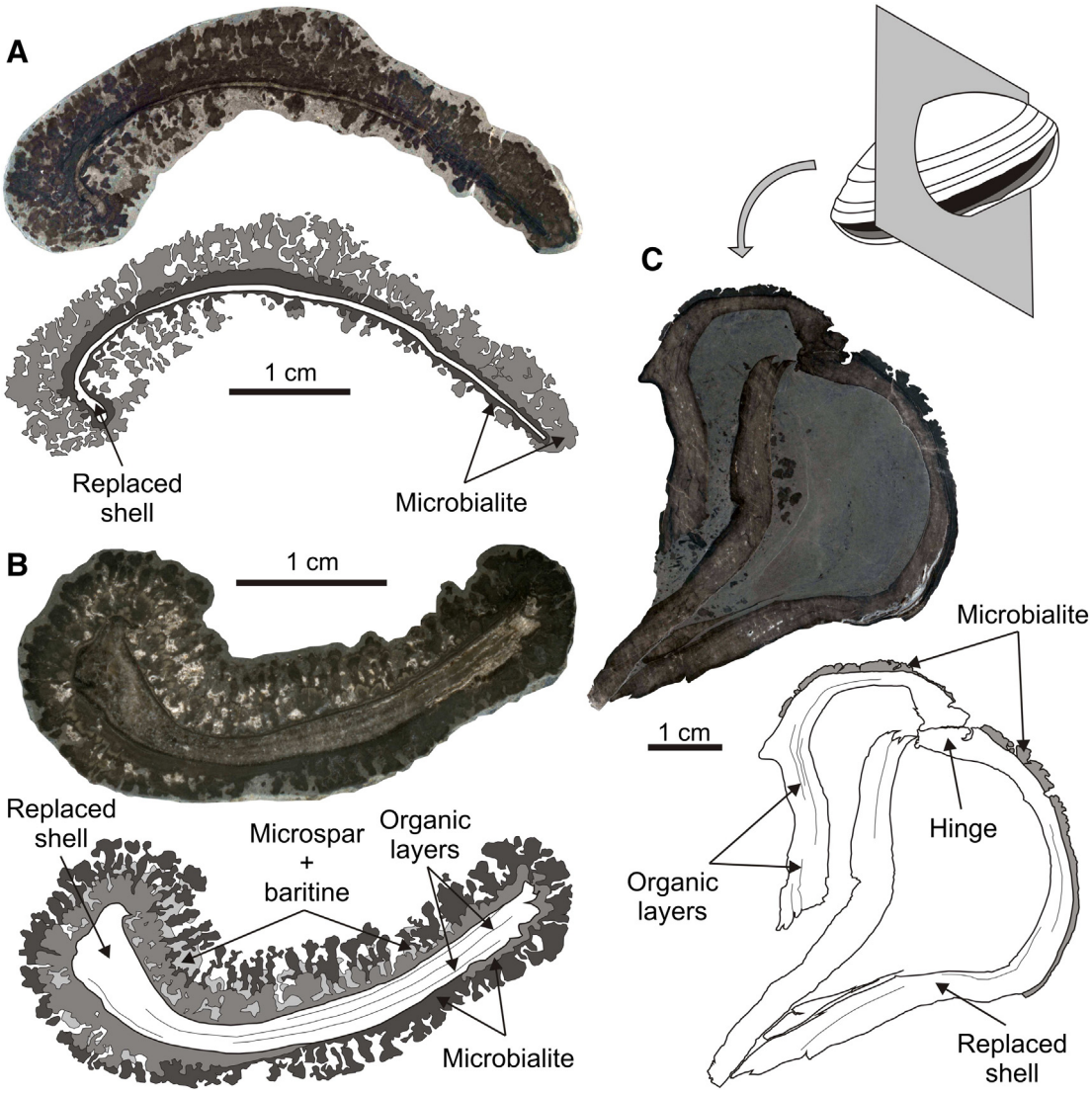

Fig. 6. Sections through microbialite crusts (Abeu section). A–B: Asymmetric growth of microbialite in isolated valves. A: Growth in the convex part of the shell. B: Growth in the concave part of the shell. C: Thin microbialite formed on the umbonal area of an articulated and fractured bivalve.

are formed by filaments of uniform thickness close to 10 μm. Other oncoids with plant or stromatolite remains acting as their cores were recovered from the same levels of the outcrop. In addition, a level represented by a 5-cm-thick microbialite mat extends for 35 cm. Such true stromatolites consist of several laminae with a slightly branched, columnar texture.

4.2.2. The Huerres section record

Common articulated bivalves show a thick microbialite cover (up to 2 cm) (Fig. 8). As with the Abeu section oncoids, the microbialite growths consist of flat or slightly wavy thin laminations, changing to domal and pseudocolumnar branched forms (Fig. 9A). This sequence is repeated several times, with festooned laminations occurring towards the external surface, and textures with open fan shapes composed of dark, radially orientated micrite filaments that branch upwards (Fig. 9B). Both the primary porosity and the tendency to branch increase towards the external part of the oncoids (Fig. 9A). These textures are similar to those described by Arenas et al. (2007, 2015) in continental Palaeogene and Jurassic oncoids, respectively.

The internal microbialite microstructure consists of a dark, flat or slightly wavy thin lamination, with a tendency to become microcolumnar and slightly branched, and with alternating dark and light microbands (Fig. 9C). Some specimens show variation in the thickness of the internal microbialite, from approximately 1 mm at the umbo up to 1 cm at the commissure (Fig. 8A, B).

In the umbonal area, the external microbialite is six times thicker than its internal counterpart. At the commissure, however, it is only three times thicker (Fig. 8A). Other samples show an internal microbialite of relatively uniform thickness of up to 1 cm (Fig. 8C).

The shell was dissolved completely during diagenesis after the first microbialite growth (external and internal). The void resulting from this dissolution was unstable and led to collapse. Where the collapse of the shell was complete, the site of the original shell can be identified because the microbialite grew in two opposite directions, and the boundary between external and internal microbialites coincides with the location of the original shell (Fig. 8C). This collapse process has been described by Leinfelder and Hartkopf-Fröder (1990) and Astibia et al. (2012) in Tertiary and Cretaceous oncoids, respectively.

However, some specimens did not collapse, and barite grew in the gap left by the dissolved shell as well as in the interior of the articulated specimens. The barite crystals are euhedral (up to 1.5 cm long; Fig. 9D) and radially distributed (Fig. 8B). The space left by the original shell was

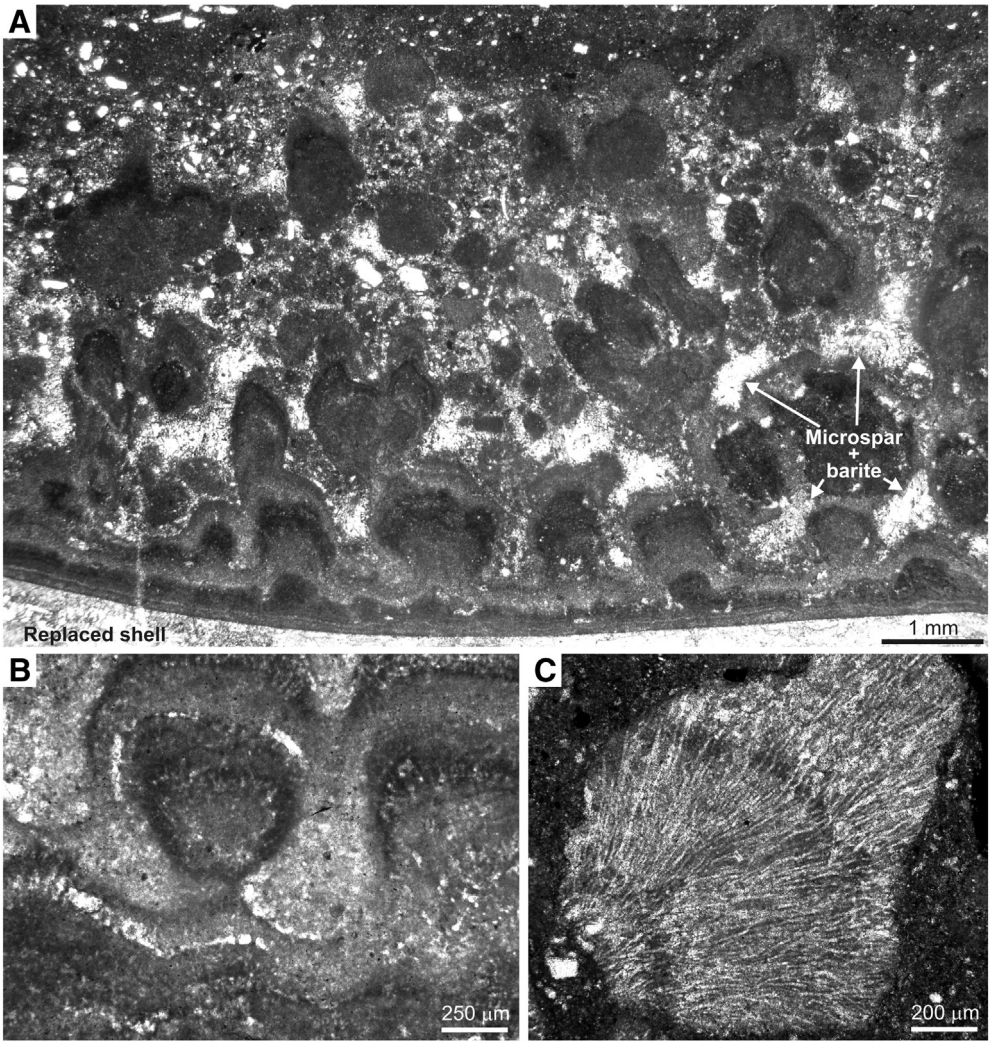

Fig. 7. Microscopic images of microbialite (Abeu section). A: Microbialite crust on a replaced bivalve shell (single valve). B: Domes developed on the umbonal area zone of an articulated bivalve. C: Cluster of isolated cyanobacterial filaments in the micritic matrix.

filled with white sparry calcite (crystals 1.5 cm long), preserving its shape. Moreover, the white calcite extends to the interior of the articulated specimens, replacing the internal microbialite and partially replacing the micrite infilled with barite. In some cases, white calcite did not fill the interior of the articulated specimens completely, and the space was filled with pink sparry calcite of a very similar texture to the white calcite, but with many barite inclusions (Fig. 8A).

4.3. Trace elements and TOC geochemistry

4.3.1. Replaced shells

The replaced shells, observed using a microprobe with a backscatter detector, consist of a mosaic of irregular crystals 5–10 µm in length. XRD revealed the presence of calcite, but not of aragonite. However, the several grey tones observed with the backscatter detector indicate considerable compositional variation in each crystal, the result of differences in the way the original aragonite was replaced. A backscatter-detected dark crystal was analysed and found to have a high Sr content (3399 ppm) and low Fe (443 ppm), Mg (271 ppm) and Mn (below the limit of detection) content. However, most part of this shell consists of calcite with very variable trace element contents (Fig. 10A–E). The mean Sr content of such shell is much lower than in the above mentioned dark crystal, while the values for Fe, Mg and Mn are higher (Fig. 10A–E. Table 1).

The S content in relict aragonite is low (SO_4: 383 ppm), far less than in the calcite replacing the shells (SO_4: 2283 ppm). A positive correlation was observed between Fe and Mn in the diagenetic calcite ($r^2 = 0.60$; Fig. 10E).

4.3.2. Microbialites

The Abeu and Huerres microbialites mainly differ in their Fe and Ba contents (Table 1; Fig. 10), while the external microbialites from both sections show similar Mg/Ca and Sr/Ca ratios (Table 1; Fig. 10).

The chemical composition of the Huerres external and internal microbialites was examined by microprobe analysis. Compositional profiles were plotted on either surface of the space left by the dissolved shell (now filled with white calcite, Fig. 11). Their trace element content is very different (Figs. 10, 11; Table 1): the internal microbialite contains less Mg and S and more Fe and Mn than the external one, although their Sr content is similar.

The Fe/Ca and Mn/Ca ratios of the Abeu samples follow the order microspar cement > replaced shell > microbialite (Fig. 10B, C, E). In the calcite of the Abeu samples, the Fe/Mn ratios are shell = 3.25; microbialite = 3.12 and microspar cement = 2.83, and they are much higher than in Huerres carbonates (microbialite: 0.64; microspar cement: 0.46). The Abeu and Huerres microbialites are notably enriched in sulphate (Fig. 12), and also have a relatively high TOC content of between 0.61 and 3.28 wt.%. The TOC content of the Abeu microbialites

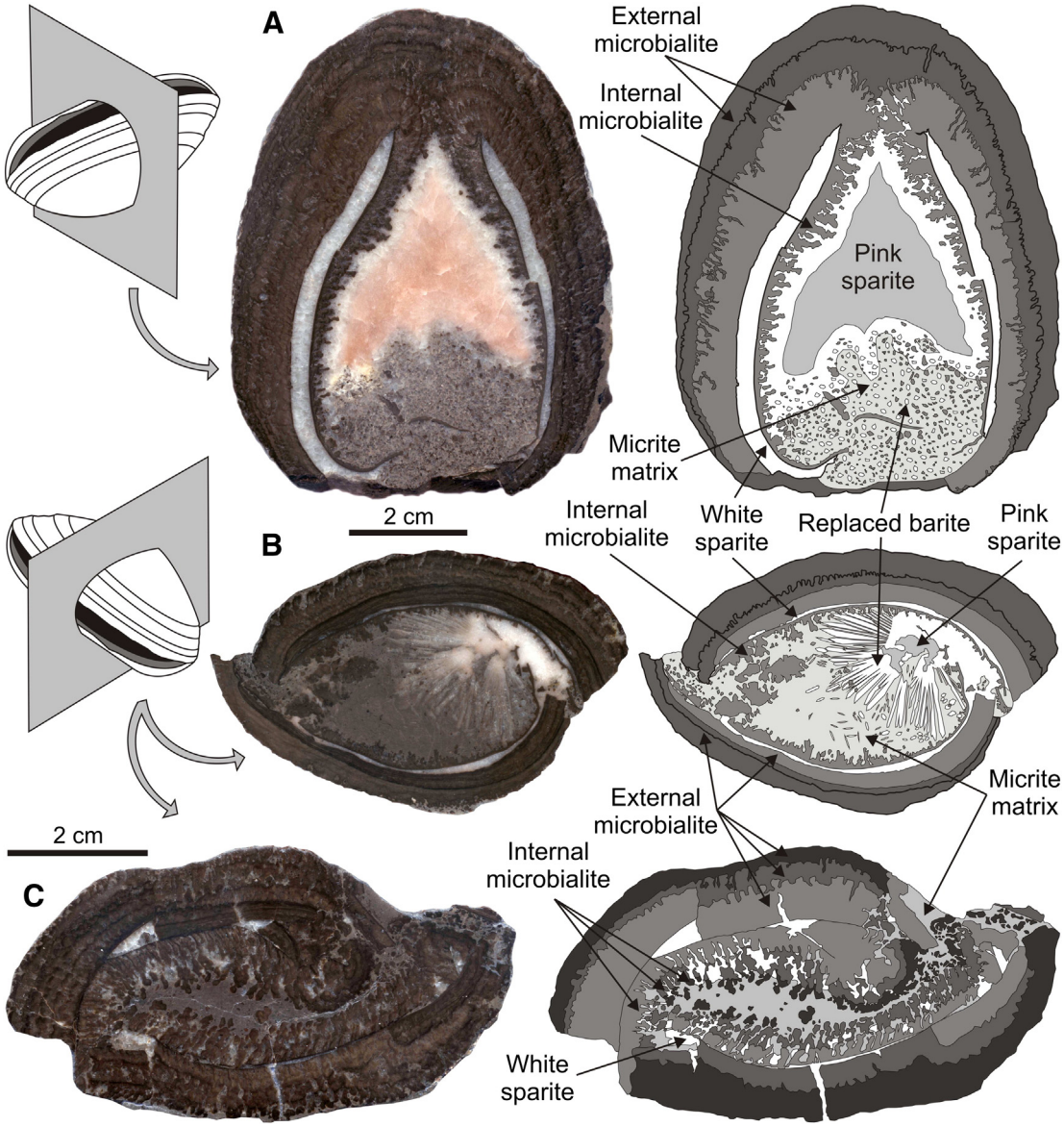

Fig. 8. Sections of bivalve microbialite crust (Huerres section). All specimens have internal and external microbialites. A–B: The external microbialite is much thicker than the internal one. A: Specimen with increased development of external and internal microbialites around the commissure of the valves. B: Specimen with increased development of internal microbialite at the commissure of the valves and of external microbialite in the umbonal area. C: Collapsed specimen with similar development of the external and internal microbialite. Note the almost complete disappearance of the bivalve shell.

(external) is substantially lower than that of their Huerres counterparts (Table 1).

4.3.3. Cements

The composition of the cement filling the primary porosity of the microbialite differs from the composition of the microbialite itself. There are some chemical differences between the Abeu and Huerres cements, but more importantly, there are differences between the cements and their respective microbialites within each section. In both, the cements incorporate more Fe and Mn than their respective microbialites, but show lower Mg, Sr and S content (Fig. 10; Table 1).

The chemical compositions of the bulk contents of the late cements (white and pink calcite) are not reliable, because these latter contain barite inclusions (especially the pink calcite). Better results were provided by microprobe analyses. The white spar fills the dissolved shells and covers the interior of the bivalves, partially replacing the internal microbialite and barite.

The Huerres white calcite does not have the same composition as the microspar that fills the porosity of the external microbialite, containing less Mg, Fe and S but more Mn and Ba than the microspar filling the primary porosity (Table 1), although their Sr values are similar (Table 1). The trace element content of the white spar is very variable (Fig. 11), and pink calcite covers the white cement in the interior of the bivalves. Despite their colour differences, their trace element content is very similar, the only important difference being Mg content, which is lower in the pink calcite (Table 1).

The different Huerres cements are richer in Mn than in Fe (Table 1). The Abeu and Huerres diagenetic spar cements contain less sulphate than the corresponding microbialites (Figs. 10, 12). The TOC concentration of the Huerres diagenetic cements is relatively high (white calcite = 2.76 wt.%; pink calcite = 1.34 wt.%), although no organic particles were observed in the sparry calcite.

4.4. Stable isotopes

$\delta^{13}C$ and $\delta^{18}O$ analyses were performed on different calcite samples of microbialite-coated shells (12 Abeu samples and 23 Huerres

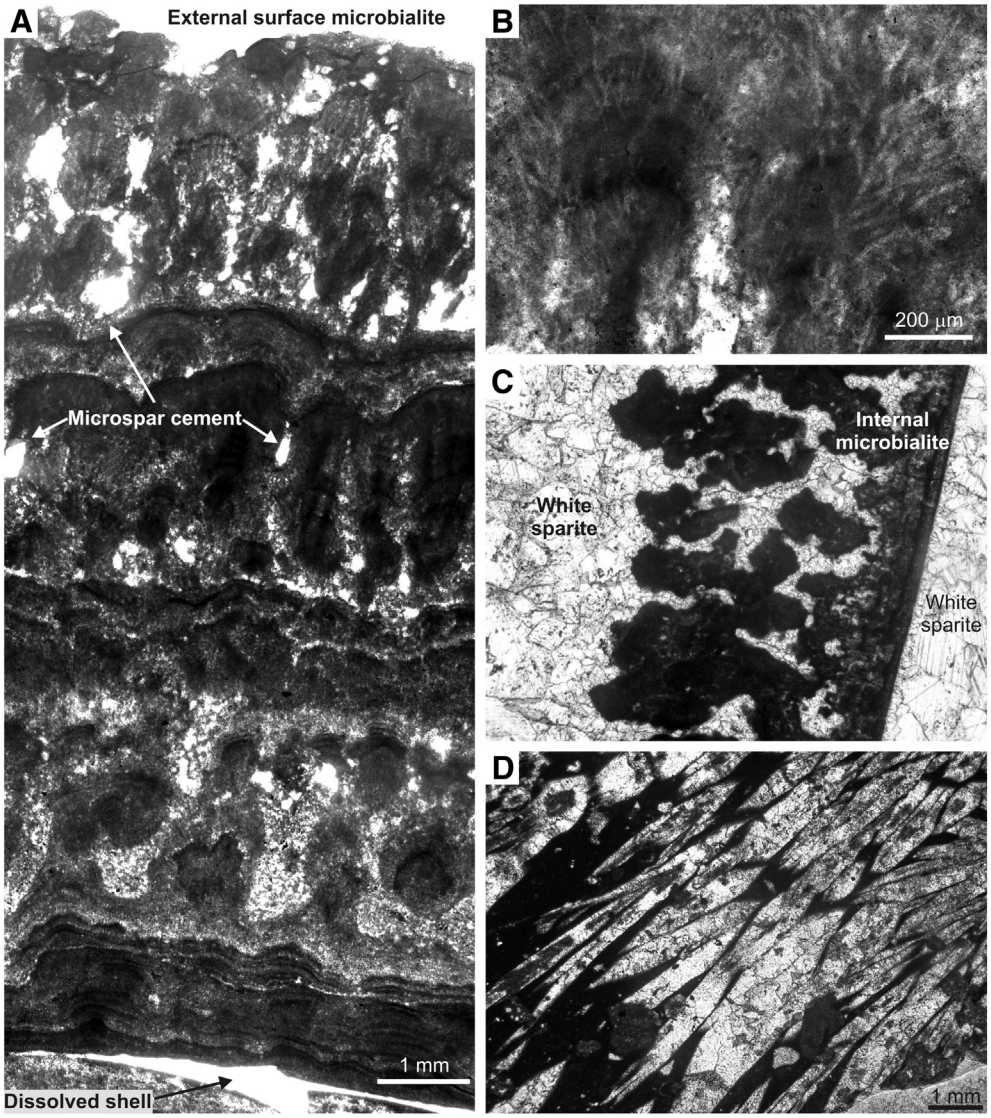

Fig. 9. Microscopic images of microbialite (Huerres section). A: External microbialite encrusting an articulated bivalve shell. B: Micrite filaments radially oriented and branched upwards in external microbialite. C: Micro-columnar, slightly branched internal microbialite, partially replaced by white calcite. D: Euhedral barite crystals in the interior of articulated specimen, also partially replaced by white calcite.

samples). Two fault fillings (one corresponding to each section) were also analysed (Table 2).

The isotope composition of the Abeu samples (replaced shells and microbialites) covered a moderate range of $\delta^{13}C$ and a wide range of $\delta^{18}O$ values. The Abeu fault filling sample had lighter carbon and oxygen than any other type of sample from this section (Table 2; Fig. 13).

The Huerres samples (microbialites and late stage cements) showed different isotope value ranges. The composition of the microbialite (11 samples) covered a narrow range of $\delta^{13}C$ and $\delta^{18}O$ (Table 2; Fig. 13), and no differences were seen between the isotope compositions of the external and internal microbialites. The carbon of late white spar (7 samples) was lighter than that measured for the corresponding microbialite and presented a narrow range. The range of oxygen isotope values was moderate (Table 2; Fig. 13), and the $\delta^{13}C$ range of the late pink spar (5 samples) was similar to that of the white calcite but lighter in oxygen. The fault filling sample analysed fell within the range of $\delta^{18}O$ for the white calcite but had heavier carbon (Table 2; Fig. 13).

Positive covariance was detected between the $\delta^{13}C$ and $\delta^{18}O$ values for the samples from each section (Fig. 13). The co-ratios of the Abeu microbialite and replaced shell samples were moderate ($r^2 = 0.60$ and 0.61, respectively); however, the co-ratio was better ($r^2 = 0.83$) when both microbialite and replaced shell were taken together. The co-variation of the Huerres microbialite samples ($r^2 = 0.59$) was similar to that of the corresponding Abeu samples, but with a much steeper slope.

5. Discussion

5.1. Palaeoenvironmental reconstruction based on the microbialite records

The thinness of the microbialite covering the articulated bivalves from Abeu (Fig. 6C) might be explained by rapid burial that did not allow for microbial growth. The microbialite on isolated valves appears better developed than that on the articulated bivalves (Fig. 6), suggesting that these valves may have lain on the bottom for a longer period of

Fig. 10. Trace elements in calcite facies. 1: Replaced shell. 2: External microbialite. 3: Internal microbialite. 4: Microspar cement in primary porosity of microbialite. 5: White spar cement in void space of dissolved bivalve shell. 6: Pink spar cement in void space inside the bivalves. 7: Replaced shell. 8: External microbialite. 9: White spar cement in void space of dissolved bivalve shell. 1–6: Microprobe data. 7–9: Bulk data: S (IR analyzer), Mg (AAS), Fe, Mn and Sr (ICP-AES).

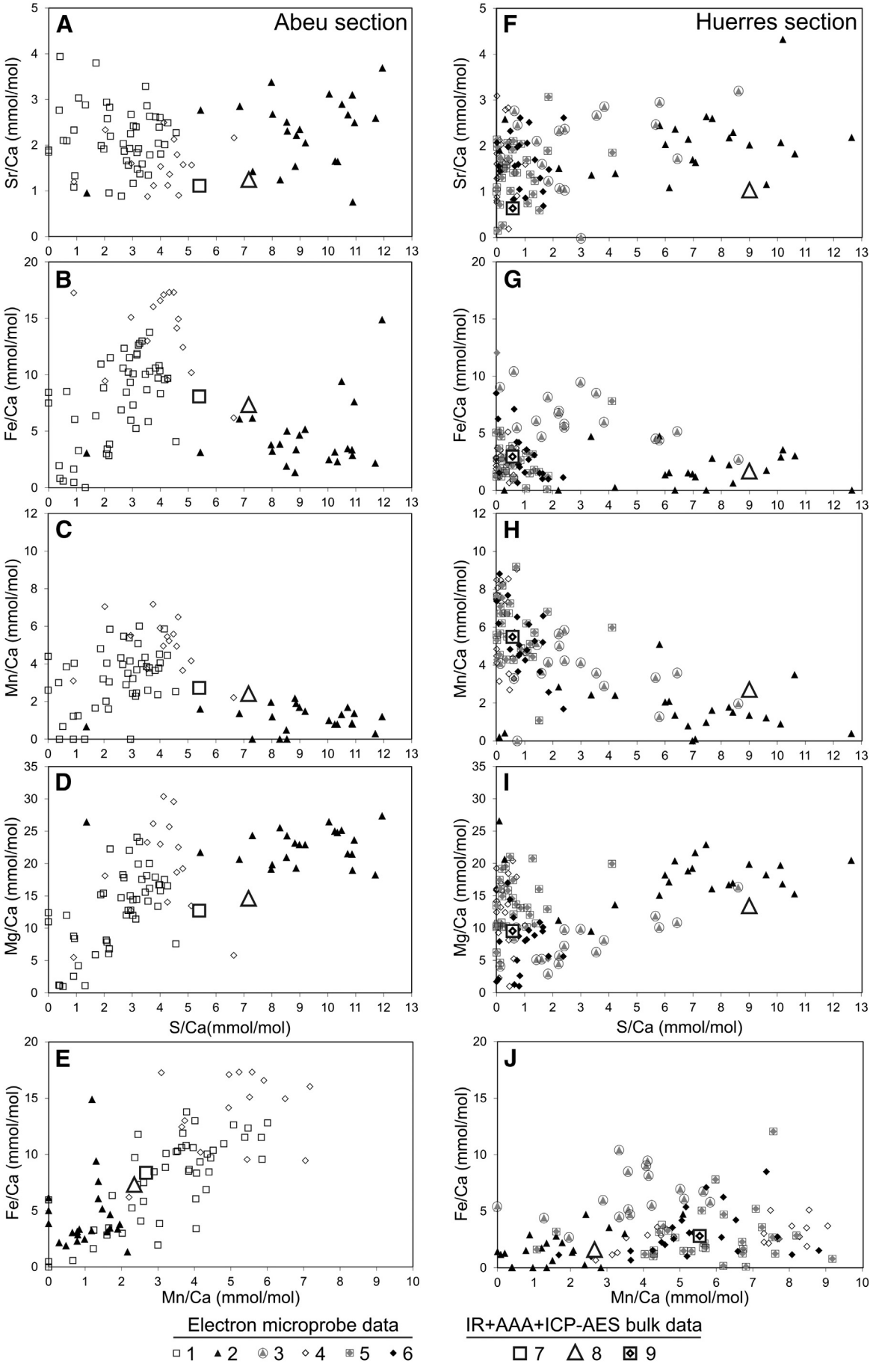
A
Abeu section
F
Huerres section
B
G
C
H
D
I
E
J
Sr/Ca (mmol/mol)
Fe/Ca (mmol/mol)
Mn/Ca (mmol/mol)
Mg/Ca (mmol/mol)
S/Ca(mmol/mol)
S/Ca (mmol/mol)
Mn/Ca (mmol/mol)
Electron microprobe data
1 2 3 4 5 6
IR+AAA+ICP-AES bulk data
7 8 9

Table 1
Trace elements and TOC compositions of replaced shells, microbialites and cements samples in the Abeu and Huerres sections.

Section	Facies	n	TOC	Ca	Mg	Fe	Mn	Sr	S	Ba
Abeu	Replaced shell	49[a]		38,04	2954	4130	1818	1829	762	269
Abeu	Replaced shell	2[b]	3,45	38,54	2883	4543	1423	972	1650	219
Abeu	External microbialite	25[a]		37,03	5125	2890	567	1838	2684	248
Abeu	External microbialite	2[b]	0,96	37,04	3155	3618	1179	954	2100	420
Abeu	Microspar cement[c]	15[a]		37,14	4320	7107	2549	1282	1196	109
Huerres	External microbialite	22[a]		37,30	4050	866	834	1684	2028	397
Huerres	External microbialite	4[b]	3,08	37,86	3140	870	1391	823	2700	38
Huerres	Internal microbialite	17[a]		36,55	1772	3267	1814	1635	902	320
Huerres	Microspar cement[c]	22[a]		37,48	2898	1451	3209	1283	77	595
Huerres	White spar cement[d]	32[a]		37,40	3091	1452	2990	1227	284	287
Huerres	Pink spar cement[e]	23[a]		38,10	1738	1585	2809	1369	264	222

TOC and Ca in wt.%, the other elements in ppm.
n = number of analyses.
[a] Microprobe.
[b] TOC and S: IR analyzer, Ca and Mg: AAS, Fe, Mn, Sr and Ba: ICP(AES).
[c] Primary porosity filler.
[d] Dissolved bivalve shell filler.
[e] Inside the bivalve filler.

time before being buried. The microbialite crust on both the convex and concave parts of the isolated valves reveals that there was sufficient energy to rework them (Leinfelder and Hartkopf-Fröder, 1990). As with several shallow infaunal bivalves, many extant unionids live partially buried, leaving only part of the umbo and posterior area of the shell above the surface. The crusts observed on the umbo of the present fossils indicate that microbialite growth began early, probably when the bivalves were still alive, or just after their death. The gypsum filling the primary porosity of the microbialite indicates that these carbonates were formed in wetland systems within a semi-arid region.

After the Huerres bivalves died, the shell interiors were not filled by micrite at an early stage (Fig. 8), unlike in the Abeu section. Following the growth of barite crystals, micritic mud penetrated the interior of the articulated specimens and covered the crystals. Precipitation of the barite was early, and the crystals may have grown before burial (just after the growth of the internal microbialite) in an evaporitic system similar to the environments observed in other lakes or tufas associated with hot springs (Arenas et al., 2000).

The Abeu and Huerres microbialites are notably enriched in sulphate (Fig. 10, Table 1) compared with other freshwater carbonates (Staudt and Schoonen, 1995), but similar to that measured in hot spring travertines (Fig. 12; Takano et al., 1980; Fouke et al., 2000). The external microbialites of Abeu and Huerres may have been formed in water with a high S content, as suggested for distal areas of hot springs (Hernández et al., 1998).

In freshwater settings, the use of Mg/Ca calcite ratios to calculate carbonate palaeotemperatures is largely unconvincing since the partitioning of Mg between calcite and water is controlled by a number of factors, including changes in the Mg/Ca and Sr/Ca ratios of the parent solutions, salinity, sulphate content, crystal growth rate, and metabolic processes (Huang and Fairchild, 2001). However, in the majority of freshwater environments, the Mg content of calcite precipitates is solely determined by the Mg/Ca and Sr/Ca ratios and water temperature (Ihlenfeld et al., 2003).

The external microbialites of the Abeu and Huerres sections show similar Mg/Ca and Sr/Ca ratios (Table 1; Fig. 10), indicating that they were formed by comparable mechanisms of micritic calcite bioprecipitation from water with a similar Mg, Sr and Ca content.

The factors that control Fe and Mn concentrations in natural waters are primarily the ambient redox conditions and the identity of the mineral phases containing the Fe and Mn. The Fe and Mn content of freshwater calcite thus reflects the prevailing water chemistry during carbonate precipitation, while increasing Fe/Ca and Mn/Ca ratios reflect a progressive reduction in the Eh (Barnaby and Rimstidt, 1989). Although the Mn content of the Abeu and Huerres microbialites is similar (Table 1; Fig. 10), the Fe content of the Huerres microbialite is much lower than that of the Abeu samples, indicating that the Huerres microbialite was formed in less reducing water and under oxygenated conditions.

Mn and Fe are oxidised at different rates, and under anoxic conditions, the reduction of Mn is more rapid than that of Fe. For this reason, higher Fe/Mn ratios indicate lower O_2 concentrations in the water column of freshwater lakes, and therefore a more reducing environment (Naeher et al., 2013). In the Abeu microbialite samples, the Fe/Mn ratio is much higher than in the Huerres microbialite, suggesting a more reducing carbonate precipitation environment for the Abeu than the Huerres section. This is also suggested by the presence of pyrite only in the Abeu microbialite.

The TOC concentration of ancient microbialites (0.01–1.10 wt.%) is generally lower than that of recent (0.8–5.0 wt.%) (McKirdy, 1976) and Holocene microbialites (1.06–4.35 wt.%) (McKirdy et al., 2010), and may occasionally be as high as 2 wt.% (Upper Permian; Słowakiewicz et al., 2013). The Abeu and Huerres microbialites have a relatively high TOC content (Table 1), indicating that part of the organic matter formed during microbialite growth was preserved. The TOC content of the Abeu external microbialites is substantially lower than that of the Huerres ones, suggesting that less organic matter was produced, or that it was consumed by bacteria.

The $\delta^{18}O$ and $\delta^{13}C$ values for the Abeu and Huerres microbialite samples (Fig. 13; Table 2) are within the range obtained for recent laminated microbialites of other fluvial and fluvial–lacustrine systems (Chafetz et al., 1991; Andrews et al., 1993; Ordóñez et al., 2005), and similar to those recorded for Palaeogene (Zamarreño et al., 1997; Arenas et al., 2007) and Jurassic sediments (Arenas et al., 2015). These values are coherent with a meteoric origin of the water, and a variable influence of soil-derived ^{12}C (Andrews, 2006). The positive covariance for the $\delta^{18}O$ and $\delta^{13}C$ of the Abeu microbialite ($r^2 = 0.60$) may be interpreted as reflecting evaporation, indicative of a longer residence time in water (Talbot, 1990; Arenas et al., 1997; Zamarreño et al., 1997; Andrews et al., 2000). Meanwhile, the positive covariance for the $\delta^{18}O$ and $\delta^{13}C$ ($r^2 = 0.59$; Fig. 13) and the steep slope recorded for the Huerres microbialite suggests intense inorganic CO_2 outgassing, typical of hydrologically open systems in fluvial environments (Talbot, 1990; Andrews, 2006; Arenas et al., 2007). The narrow range of variation for $\delta^{18}O$ (0.74‰) indicates that the effect of evaporation was much less significant than in the Abeu section, for which the $\delta^{18}O$ varied by 2.06‰. The very low $\delta^{18}O$ and $\delta^{13}C$ values for the fault fillings (−12.24 and −7.32‰, respectively) indicate that this derived from ^{16}O-enriched meteoric water with contributions of soil-derived ^{12}C. This meteoric water, which differed from the Jurassic water in which the microbialites

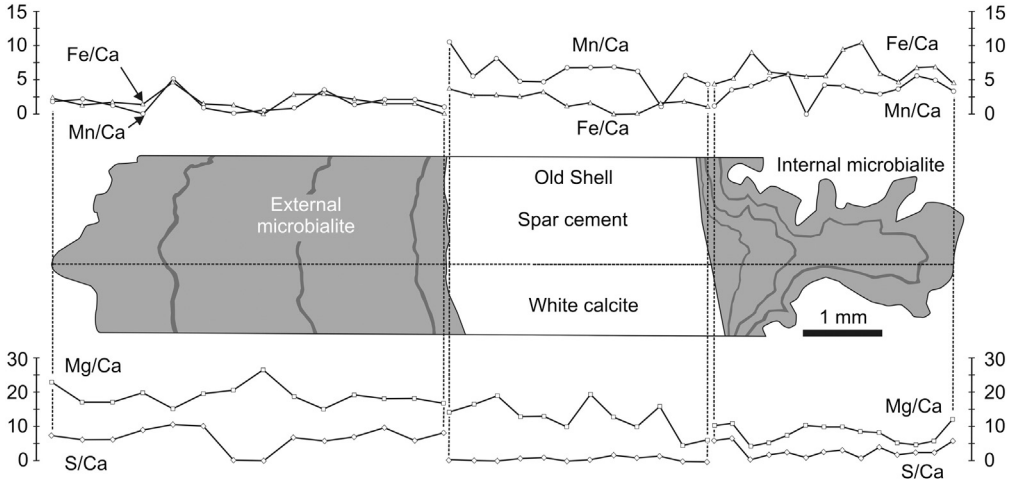

Fig. 11. Chemical profiles (Mn/Ca, Fe/Ca, Mg/Ca and S/Ca) in external and internal microbialite separated by white calcite filling the void of the dissolved bivalve shell. The profiles were drawn across the umbonal area.

were formed, entered through fractures that formed after consolidation of the sediment.

5.2. Shell replacement as tool for palaeoenvironmental reconstruction

The original aragonite of bivalve shells generally undergoes dissolution in meteoric waters, and any cement that forms is typically calcite or dolomite, depending primarily on the Mg/Ca ratio, the salinity of the diagenetic fluid and the precipitation rate (Morse et al., 1997). Meteoric diagenesis generally favours the precipitation of calcite over aragonite since the Mg/Ca ratio is usually very low in freshwater environments (Webb et al., 2007).

The distribution of trace elements in carbonates depends on the mineralogy. The aragonite lattice tends to accept ions of a larger radius than Ca, such as Sr and Ba, but the calcite lattice only accepts ions of a smaller radius, such as Mg, Fe and Mn (Graf, 1960; Bischoff and Fyfe, 1968; Treese et al., 1981). Consequently, during the replacement process, calcite incorporates more Mg, Fe and Mn and loses part of its Sr (Sandberg and Hudson, 1983; Brand, 1989).

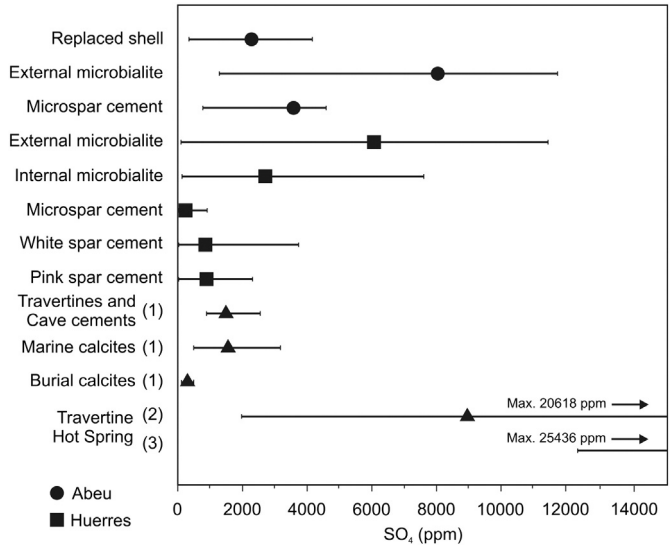

Fig. 12. Sulphate concentration ranges (horizontal bars) and average contents of replaced shell and microbialite (Abeu section; solid circles), and of external and internal microbialite and diagenetic cements (Huerres section; solid square). Bars with triangle, 1: travertine and cave cements, marine and burial calcites (Staudt and Schoonen, 1995), 2: travertine hot springs (Fouke et al., 2000), 3: travertine hot springs (Takano et al., 1980).

In replaced shells from the Abeu section, these changes can be observed by comparing the chemical composition of the sparse relict aragonite and the calcite that replaced it. The positive correlation between Fe and Mn in calcite ($r^2 = 0.60$; Fig. 10E) also reflects a simultaneous increase in both elements during shell replacement. However, the Fe, Sr, Mn and Mg content of replaced shells and microbialites are similar, suggesting that they were both formed in a short time interval, although

Table 2
Stable isotopic compositions ($\delta^{13}C$ and $\delta^{18}O$) of calcite samples from the Abeu and Huerres sections.

Sample	Locality	Facies	Calcite texture	$\delta^{13}C$ (‰V-PDB)	$\delta^{18}O$ (‰V-PDB)
AB-01	Abeu	Replaced shell	Spar	−6,26	−8,52
AB-02	Abeu	Replaced shell	Spar	−6,48	−8,48
ABX-1-C	Abeu	Replaced shell	Spar	−5,98	−8,26
ABX-2-C	Abeu	Replaced shell	Spar	−5,95	−7,86
ABX-3-C	Abeu	Replaced shell	Spar	−6,35	−8,32
ABX-7-C	Abeu	Replaced shell	Spar	−5,91	−8,12
AB-03	Abeu	External microbialite	Micrite	−6,03	−7,81
AB-04	Abeu	External microbialite	Micrite	−4,93	−6,14
AB-05	Abeu	External microbialite	Micrite	−4,67	−5,72
ABX-1-M	Abeu	External microbialite	Micrite	−5,13	−6,55
ABX-2-M	Abeu	External microbialite	Micrite	−5,45	−6,79
ABX-3-M	Abeu	External microbialite	Micrite	−5,65	−6,00
ABX-F	Abeu	Fault filling	Spar	−7,32	−12,24
HU-10	Huerres	External microbialite	Micrite	−6,95	−4,97
HU-11	Huerres	External microbialite	Micrite	−6,94	−5,19
HU-14	Huerres	External microbialite	Micrite	−6,39	−4,58
HU-15	Huerres	External microbialite	Micrite	−6,12	−4,63
HU-20	Huerres	External microbialite	Micrite	−6,01	−4,60
HU-21	Huerres	External microbialite	Micrite	−6,11	−4,61
HU-22	Huerres	External microbialite	Micrite	−6,99	−5,22
HU-23	Huerres	External microbialite	Micrite	−6,29	−4,48
HU-24	Huerres	Internal microbialite	Micrite	−6,19	−5,00
HU-13	Huerres	Internal microbialite	Micrite	−5,85	−4,68
HU-17	Huerres	Internal microbialite	Micrite	−6,19	−4,62
HU-07	Huerres	White spar cement	Spar	−8,26	−6,19
HU-08	Huerres	White spar cement	Spar	−8,12	−7,05
HU-09	Huerres	White spar cement	Spar	−8,26	−7,84
HUX-1-B	Huerres	White spar cement	Spar	−8,24	−6,77
HUX-2-B	Huerres	White spar cement	Spar	−7,89	−6,69
HUX-3-B	Huerres	White spar cement	Spar	−8,26	−6,14
HUX-4-B	Huerres	White spar cement	Spar	−7,71	−7,03
HU-06	Huerres	Pink spar cement	Spar	−7,81	−9,14
HUX-1-R	Huerres	Pink spar cement	Spar	−8,07	−8,82
HUX-2-R	Huerres	Pink spar cement	Spar	−7,64	−9,16
HUX-5-R	Huerres	Pink spar cement	Spar	−7,62	−8,71
HUX-10-R	Huerres	Pink spar cement	Spar	−8,00	−10,21
HUX-F	Huerres	Fault filling	Spar	−6,99	−6,81

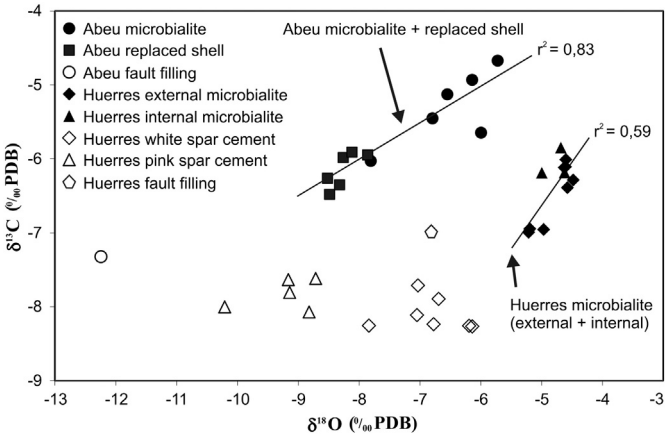

Fig. 13. Stable isotopic composition ($\delta^{13}C$ vs. $\delta^{18}O$) of replaced shells, microbialites and cements samples (Table. 2) in Abeu and Huerres sections.

not at the same time because the replaced shells contain much less sulphur than the microbialites (Fig. 10A–D).

The organic matter content of bivalve shells varies from species to species, but does not generally exceed 5 wt.% (Bayer et al., 2013). The literature contains very little on TOC values for either recent or fossil bivalve shells (up 2 wt.% in modern freshwater bivalves has been suggested by Jurkiewicz-Karnkowska, 2005). The replaced shells preserve a large amount of organic matter derived from the original nacre and the organic layers inside it. Assuming that some 50% of the organic matter was lost during replacement (Sandberg and Hudson, 1983), the Abeu section bivalves must, in their day, have contained a high percentage of organic matter in the shell (TOC ~ 7 wt.%). The S bulk content in the shells is even higher, indicating that a portion of the S belongs to the organic matter contained within the shell but outside the calcite.

Assuming isotopic equilibrium between the shell and the ambient water, variations in $\delta^{18}O$ and $\delta^{13}C$ in bivalve shells reflect both the oxygen and carbon isotope ratios of the ambient water and the temperature during biomineralisation (Yan et al., 2014). Although the isotope composition of the Abeu replaced shells is similar to that of some present-day freshwater bivalves (Yan et al., 2009), it is probable that it was modified after replacement. During diagenetic transformation, $\delta^{18}O$ and $\delta^{13}C$ concentrations decrease (Sandberg and Hudson, 1983; Brand, 1989), so the isotope composition of the original aragonite shells in the Abeu section may have been similar to that recorded for the microbialite (Fig. 13). In fact, the high positive covariance of $\delta^{18}O$ and $\delta^{13}C$ of the Abeu microbialite and replaced shells ($r^2 = 0.83$; Fig. 13) suggests that replacement of the aragonite shell occurred shortly before microbialite growth in a scenario dominated by evaporation, indicative of a long residence time in the water (Talbot, 1990; Arenas et al., 1997; Zamarreño et al., 1997; Andrews et al., 2000).

5.3. Influence of growth rate on microbialite geochemistry

The thickest growth of the Huerres microbialite is seen at the aperture of the valves, while it is thin in the umbonal area. This indicates that after the death of the animals, some of them lay on the bottom with the posterior area facing upwards, with the thickest growth of microbialite occurring in this most illuminated area (Fig. 8A, B). The progressive reduction in the carbonate dissolved in water inside the shell of non-collapsed bivalves should produce a lower rate of calcite precipitation in relation to the growth of external microbialite. However, this is highly unlikely because the shell would need to remain completely isolated from the outside, and in the early stages of microbialite growth, the bivalve would be open (Fig. 8A). Therefore, the thinness of the internal microbialite probably indicates that little light reached the interior of the shell, reducing the growth of the internal microbialite coating. The appreciable development of internal microbialite in collapsed shells (Fig. 8C) might be explained by sunlight entering through numerous post-collapse fractures.

The internal microbialite was developed on the original aragonite shell or on the replacement calcite, which was subsequently dissolved. The texture of some samples shows that the precipitation rate for the internal microbialite was lower than that of the external one (Fig. 8A, B). Such differences may be the result of the amount of light reaching the shell. More would have reached the exterior part, stimulating the activity of cyanobacteria which, through their photosynthesis, produced the microbialite calcite.

The internal microbialite contains less Mg and S and more Fe and Mn than the external one, while their Sr content is similar (Fig. 11). Since the interior and exterior temperatures of the bivalves were identical, this reduction in Mg and S is probably related to the low precipitation rate of the calcite in the shell interior. This slow growth rate may have allowed for a greater selection of elements dissolved in the water, preventing the incorporation of sulphate, an ion that is considerably larger than the carbonate ion and tetrahedral rather than planar in form (Staudt and Schoonen, 1995).

The distribution coefficients for Mn and Fe in calcite are not only influenced by temperature (Bodine et al., 1965), but also by the precipitation rate (Mucci, 1988). For example, Lorens (1981) has shown that the distribution coefficient for Mn varies from 5 at rapid precipitation rates to almost 70 at very slow rates. One might infer that the distribution coefficients for Fe would show a similar behaviour. The low growth rate of the internal microbialite might be responsible for the much stronger incorporation of Fe and Mn into the carbonate (Figs. 10, 11; Table 1). Moreover, the Fe/Mn ratio of the internal microbialite (1.83) is greater than that recorded for any other Huerres carbonate, suggesting that a slightly more reducing micro-environment reigned inside the shell than outside during precipitation of the internal microbialite.

5.4. Diagenetic alteration of microbialites

The Abeu samples appear to have been affected solely by early diagenesis, as evidenced by microspar filling in the primary porosity (Fig. 7A) and the replacement of the shell by calcite (Fig. 5H, I). In contrast, the Huerres samples were affected both by early (microspar filling the primary porosity; Fig. 9A) and late diagenesis (white and pink spar; Fig. 8). Although microspar cements could be early, and formed from the same water in which the microbialite precipitated (Pentecost, 2005), the reduction in Mg and Sr suggests that the cements were formed after burial. Furthermore, their Fe and Mn concentrations are higher than in the microbialites (Table 1, Fig. 10), indicating a clear oxygen deficit.

The Abeu and Huerres diagenetic microspar cements contain less sulphate than the corresponding microbialites (Figs. 10, 12). This suggests that compared with the latter, they precipitated in more reducing subsurface environments with lower sulphate concentrations (Staudt and Schoonen, 1995). The cement with the highest sulphate content fills the porosity of the Abeu microbialite (Fig. 10, Table 1), and its sulphate content is similar to that of the calcite that replaced the original aragonite shell (Fig. 12), indicating that the filling was early, probably coetaneous with shell replacement. The early and late Huerres cements are richer in Mn than Fe (Fig. 10), suggesting that they were formed in very well oxygenated water.

The high TOC concentration in the Huerres diagenetic cements (Table 1) and the absence of organic particles suggest that the organic matter is probably in the form of humic acid, and was both adsorbed onto the calcite surface and incorporated into the calcite lattice during crystallisation (Chalmin et al., 2013). The organic matter of these cements may have come from plant decomposition and would have been transported downwards through the fractures into the interior porosity of the bivalves where it precipitated. Alternatively, it could have come from thermal maturation of the organic matter in the sediments above the bivalves.

The $\delta^{13}C$ values for late stage Huerres cements (white and pink spar calcite) suggest a meteoric origin of the water and an influence of soil-derived ^{12}C. However, the $\delta^{18}O$ and $\delta^{13}C$ values are lighter than those obtained for the microbialite (Table 2; Fig. 13), suggesting that the cements were formed after burial. The fault fillings have the same oxygen value (−6.81‰) as the mean recorded for the white calcite (−6.82‰), although this latter has slightly heavier carbon. This indicates that the meteoric water penetrated the surface via fractures after sediment consolidation, with the white spar calcite precipitating both in fractures and bivalve voids. The light carbon is related to an increased contribution of soil-derived ^{12}C from above the sediment column. The later pink cements were also formed from meteoric waters but have lighter oxygen. This indicates a similar contribution of soil-derived ^{12}C but with the intervention of different meteoric water.

6. Conclusions

The Abeu and Huerres carbonate deposits were formed in different Jurassic continental environments, but in water presenting similar geochemical properties, for example Mg/Ca and Sr/Ca content. Sulphur enrichment of microbialite crusts in both deposits indicates that the water in which the bivalves lived came from hot springs.

The Abeu carbonate deposits in which the bivalves were found reflect a freshwater carbonate wetland–pond system located in local topographic lows controlled by small synsedimentary faults. The gypsum and barite filling of the primary porosity of the Abeu microbialites indicates that these oncoids were formed in wetland systems within a semi-arid region. Isotope values ($\delta^{18}O$ and $\delta^{13}C$) for the replaced shells and microbialite also reveal the existence of a semi-arid environment dominated by evaporation. This was probably one of several small, isolated ponds in which the water remained stagnant (hydrologically closed) for long periods of time. The high Fe/Mn ratio of Abeu microbialites indicates that these ponds had a low concentration of O_2. The thinness of the microbialite on articulated Abeu shells indicates that the bivalves were buried quickly and received very little sunlight. The preferential growth seen in the umbonal area suggests that microbialites were formed on bivalves while these were still alive (or very soon after their death).

In contrast to the Abeu section, the weak correlation between isotope values ($\delta^{18}O$ and $\delta^{13}C$) for the Huerres microbialites and the slight variation in $\delta^{18}O$ together indicate that these oncoids were formed in open water systems in which degassing predominated over evaporation. The low Fe/Mn ratio suggests that the agitation of water produced good oxygenation, as well as CO_2-degassing. In the non-collapsed bivalves from the Huerres section, internal microbialite grew much more slowly than its external counterpart due to a deficit of sunlight in the shell interior. Based on the incorporation of trace elements, an estimate can be made of the influence of microbialite growth rate (which was six times higher for the external microbialite). The internal microbialite incorporated less Mg and S and more Fe and Mn than the external one, while their Sr content was the same. A comparison between the trace elements of early cements from the Abeu and Huerres sections and their respective microbialite crusts shows that the cements were formed after burial, in S-low oxygenated waters. Based on isotopic and trace element composition, the Huerres late cements were also formed after burial, in meteoric waters influenced by ^{12}C derived soils.

Acknowledgement

We thank to Luis Alfonso Fernández Pérez for his help in the fieldwork. Alfredo Fernández Larios is greatly acknowledged for assistance in the EMP analyses. We thank Jesus Reyes and Juan Antonio Martín Rubí (Tres Cantos Laboratory, IGME) for their support and assistance in the chemical and DRX analyses. This is a contribution to the MINECO-Excelencia CGL2013-42643-P, CGL2012-33281 Ministry of Economy and Competitiveness, IGCP 632 project "Continental Crises of the Jurassic: Major Extinction events and Environmental Changes within Lacustrine Ecosystems" and it is partially funded by the Instituto Geológico y Minero de España (IGME, Government of Spain). Photographs of fossils were produced by the Paleontological Photography Service at the University of Zaragoza (Zarela Herrera). We are grateful to Dr. Dunagan (University of Tennessee), Prof. F.T. Fürsich (University of Erlangen) and an anonymous reviewer for the review of the manuscript. We thank the "Gabinete Lingüístico Centro Superior de Idiomas Modernos" (Universidad Complutense de Madrid) for revising the English style of this manuscript.

References

Alonso, J.L., Gallastegui, J., García-Ramos, J.C., Poblet, J., 2009. Estructuras mesozoicas y cenozoicas relacionadas con la apertura y cierre parcial del Golfo de Vizcaya (Zona Cantábrica-Asturias). Atlantic Iberian Margin, Guía de Campo, Oviedo 6th Symp. (18 pp.).

Andrews, J.E., 2006. Palaeoclimatic records from stable isotopes in riverine tufas: synthesis and review. Earth Sci. Rev. 75, 85–104.

Andrews, J.E., Riding, R., Dennis, P.F., 1993. Stable isotopic compositions of recent freshwater cyanobacterial carbonates from the British Isles: local and regional environmental controls. Sedimentology 40, 303–314.

Andrews, J.E., Pedley, M., Dennis, P.F., 2000. Palaeoenvironmental records in Holocene Spanish tufas: a stable isotope approach in search of reliable climatic archives. Sedimentology 47, 961–978.

Arenas, C., Casanova, J., Pardo, G., 1997. Stable-isotope characterization of the Miocene lacustrine systems of Los Monegros (Ebro Basin, Spain): palaeogeographic and palaeoclimatic implications. Palaeogeogr. Palaeoclimatol. Palaeoecol. 128, 133–155.

Arenas, C., Gutiérrez, F., Osácar, C., Sancho, C., 2000. Sedimentology and geochemistry of fluvio–lacustrine tufa deposits controlled by evaporite solution subsidence in the central Ebro Depresion, NE Spain. Sedimentology 47, 883–909.

Arenas, C., Cabrera, L., Ramos, E., 2007. Sedimentology of tufa facies and continental microbialites from the Palaeogene of Mallorca Island (Spain). Sediment. Geol. 197, 1–27.

Arenas, C., Piñuela, L., García-Ramos, J.C., 2015. Climatic and tectonic controls on carbonate deposition in syn-rift siliciclastic fluvial systems: a case of microbialites and associated facies in the Late Jurassic. Sedimentology 62, 1149–1183.

Astibia, H., López-Martínez, N., Elorza, J., Vicens, E., 2012. Increasing size and abundance of microbialites (oncoids) in connection with the K/T boundary in nonmarine environments in the South Central Pyrenees. Geol. Acta 10, 209–226.

Aurell, M., Robles, S., Bádenas, B., Rosales, I., Quesada, S., Meléndez, G., García-Ramos, J.C., 2003. Transgressive–regressive cycles and Jurassic palaeogeography of northeast Iberia. Sediment. Geol. 162, 239–271.

Banner, J.L., 1995. Application of the trace element and isotope geochemistry of strontium to studies of carbonate diagenesis. Sedimentology 42, 805–824.

Barnaby, R.J., Rimstidt, J.D., 1989. Redox conditions of calcite cementation interpreted from Mn and Fe contents of authigenic calcite. Geol. Soc. Am. Bull. 101, 795–804.

Barrón, E., 2010. Las series fluviales del Jurásico superior (Formación Vega). Palinología. In: García-Ramos, J.C. (Ed.), V Congreso del Jurásico de España, Guía de campo, excursión A. Museo del Jurásico de Asturias, Colunga, pp. 64–68.

Bayer, M.S., Colombo, F., De Vincentis, N.S., Duarte, G.A., Bolmaro, R., Gordillo, S., 2013. Cryptic diagenetic changes in Quaternary aragonitic shells: a textural, crystallographic, and trace-element study on *Amiantis purpurata* (Bivalvia) from Patagonia, Argentina. Palaios 28, 438–451.

Bischoff, J.L., Fyfe, W.S., 1968. Catalysis, inhibition and the calcite–aragonite problem; [Part] I, the aragonite–calcite transformation. Am. J. Sci. 266, 65–79.

Bodine, M.W., Holland, H.D., Borcisk, M., 1965. Co-precipitation of manganese and strontium with calcite. In: Stemprock, M., Rieder, M. (Eds.), Symposium on Problems of Postmagmatic Ore Deposition, Prague. 2, pp. 401–406.

Bosence, D., 2012. Mesozoic, syn-rift, non-marine, microbialites from the Wessex Basin, UK. AAPG Hedberg Conference. Microbial Carbonate Reservoir Characterization. pp. 1–3.

Brand, U., 1989. Aragonite–calcite transformation based on Pennsylvanian molluscs. Geol. Soc. Am. Bull. 101, 377–390.

Burton, E.A., Walter, L.M., 1991. The effects of P_{CO2} and temperature on magnesium incorporation in calcite in seawater and $MgCl_2$–$CaCl_2$ solutions. Geochim. Cosmochim. Acta 55, 777–785.

Cabaleri, N.G., Benavente, C.A., Monferran, M.D., Narváez, P.L., Volkheimer, W., Gallego, O.F., Do Campo, M.D., 2013. Sedimentology and palaeontology of the Upper Jurassic Puesto Almada Member (Cañadón Asfalto Formation, Fossati sub-basin), Patagonia Argentina: palaeoenvironmental and climatic significance. Sediment. Geol. 296, 103–121.

Carroll, M., Romanek, C.S., 2008. Shell layer variation in trace element concentration for the freshwater bivalve *Elliptio complanata*. Geo-Mar. Lett. 28, 369–381.

Carter, J.G., Tevesz, M.J.S., 1978. Shell microstructure of a Middle Devonian (Hamilton Group) bivalve fauna from central New York. J. Paleontol. 52, 859–880.

Chafetz, H., Rush, P.F., Utech, N.M., 1991. Microenvironmental controls on mineralogy and habit of $CaCO_3$ precipitates: an example from an active travertine system. Sedimentology 38 (1), 107–126.

Chalmin, E., Perrette, Y., Fanget, B., Susini, J., 2013. Investigation of organic matter entrapped in synthetic carbonates — a multimethod approach. Microsc. Microanal. 19, 132–144.

Delvene, G., Munt, M., Royo-Torres, R., Cobos, A., Alcalá, L., 2013a. Late Jurassic–Early Cretaceous freshwater bivalves from *Turiasaurus riodevensis* bearing strata of Teruel (Spain). Span. J. Palaeontol. 28, 161–172.

Delvene, G., Lozano, R.P., Munt, M., Piñuela, L., García-Ramos, J.C., 2013b. In: Álvarez-Vázquez, C., López Rodríguez, I. (Eds.), Unionoids (Bivalvia) and their Associated Microbialites from the Late Jurassic of Asturias (Spain). Jorn. Soc. Esp. Paleontol., Córdoba XXIX, pp. 147–148.

Delvene, G., Munt, M., Piñuela, L., García-Ramos, J.C., 2015. New Taxa of the Unionida (Bivalvia) from the Kimmeridgian (Late Jurassic) of the Dinosaur Coast (Asturias, Spain), and their Palaeobiogeographical Implications for the Non-marine Mesozoic Fauna of Europe (in press).

Djamali, M., Soulié-Märsche, I., Esu, D., Gliozzi, E., Okhravi, R., 2006. Palaeoenvironment of a Late Quaternary lacustrine–palustrine carbonate complex: Zarand Basin, Saveh, central Iran. Palaeogeogr. Palaeoclimatol. Palaeoecol. 237, 315–334.

Dunagan, S., 2007. Recognition of Late Jurassic carbonate wetlands and lakes from the Morrison Formation (Colorado). Geol. Soc. Am. Abstr. Programs 39, 606.

Dunagan, S.P., Turner, C.E., 2004. Regional paleohydrologic and paleoclimatic settings of wetland/lacustrine depositional systems in the Morrison Formation (Upper Jurassic), Western Interior, USA. Sediment. Geol. 167, 269–296.

Dupraz, C., Reid, R.P., Braissant, O., Decho, A.W., Norman, R.S., Visscher, P.T., 2008. Processes of carbonate precipitation in modern microbial mats. Earth-Sci. Rev. 96, 141–162.

Fouke, B.W., Farmer, J.D., Des Marais, D.J., Pratt, L., Sturchio, N.C., Burns, P.C., Discipulo, M.K., 2000. Depositional facies and aqueous-solid geochemistry of travertine-depositing hot springs (Angel Terrace, Mammoth Hot Springs, Yellowstone National Park, U.S.A.). J. Sediment. Res. 70, 565–585.

Galiana, R., 1979. Nuevos yacimientos malacológicos en el Terciario continental de Mallorca. Bol. Soc. Hist. Nat. Baleares 23, 117–126.

García-Ramos, J.C., Gutiérrez Claverol, M., 1995. La cobertera Mesozoico-Terciaria. In: Aramburu, C., Bastida, F. (Eds.), Geología de Asturias. Ed. Trea. Gijón., pp. 81–94.

García-Ramos, J.C., Piñuela, L., Uzkeda, H., Poblet, J., Bulnes, M., Alonso, J.L., Suárez Vega, L.C., 2010a. Travertinos ricos en oncoides asociados a paleomanantiales y lagos efímeros próximos a fallas sinsedimentarias en el Jurásico Superior de Asturias. In: Ruiz-Omeñaca, J.I., Piñuela, L., García-Ramos, J.C. (Eds.), Comunicaciones del V Congreso del Jurásico de España. Museo del Jurásico de Asturias, Colunga, pp. 83–91.

García-Ramos, J.C., Aramburu, C., Piñuela, L., 2010b. Las series fluviales del Jurásico superior (Formación Vega). Descripción de la serie y ambientes sedimentarios. In: García-Ramos, J.C. (Ed.), V Congreso del Jurásico de España, Guía de campo, Excursión A. Museo del Jurásico de Asturias, Colunga, pp. 56–63.

García-Ramos, J.C., Piñuela, L., Rodríguez-Tovar, F.J., 2011. Introduction to the Jurassic of Asturias. XI International Ichnofabric Workshop, Museo del Jurásico de Asturias, Colungapp. 3–8.

Gradzinski, M., Tyszka, J., Uchman, A., Jach, R., 2004. Large microbial foraminiferal oncoids from condensed Lower–Middle Jurassic deposits: a case study from the Tatra Mountains, Poland. Palaeogeogr. Palaeoclimatol. Palaeoecol. 213, 133–151.

Graf, D.L., 1960. Geochemistry of carbonate sediments and sedimentary carbonate rocks. Part III: Minor Element DistributionIllinois State Geol. Surv. Circ. 301 (71 pp.).

Gray, W., Holmes, J., Shevenell, A., 2014. Evaluation of foraminiferal trace element cleaning protocols on the Mg/Ca of marine ostracod genus *Krithe*. Chem. Geol. 382, 14–23.

Gutierrez, K., Sheldon, N.D., 2012. Paleoenvironmental reconstruction of Jurassic dinosaur habitats of the Vega Formation, Asturias, Spain. Geol. Soc. Am. Bull. 124, 596–610.

Heim, A., 1916. Monographie der Churfürsten-Matt stock-Gruppe. 3. LithogenesisBeitr. Geol. Karte Schweiz, N.F. 20 pp. 369–662.

Hendry, J.P., Perkins, W.T., Bane, T., 2001. Short-term environmental change in a Jurassic lagoon deduced from geochemical trends in aragonite bivalve shells. Geol. Soc. Am. Bull. 113 (6), 790–798.

Hernández, J.M., Diéguez, C., Pujalte, V., Robles, S., Wright, V.P., 1998. Reconocimiento de acumulaciones travertínicas fósiles en la Fm. Aguilar (Kimmeridgiense-Berriasiense de Palencia y Burgos): implicaciones paleoecológicas y paleohidrológicas. Geogaceta 24, 167–170.

Hernández Gómez, J.M., 2000. Sedimentología, paleogeografía y relaciones tectónica/sedimentación de los sistemas fluviales, aluviales y palustres de la cuenca rift de Aguilar (Grupo Campoo, Jurásico superior-Cretácico inferior de Palencia, Burgos y Cantabria). PhD ThesisDepto. Estratigr. Paleontol. Fac. Ciencias. Univ. País Vasco, España (324 pp.).

Hiscott, R.N., Wilson, R.C.L., Gradstein, F.M., Pujalte, V., García-Mondéjar, J., Boudreau, R.R., Wishart, H.A., 1990. Comparative stratigraphy and subsidence history of Mesozoic rift basins of North Atlantic. AAPG Bull. 74, 60–76.

Huang, Y.M., Fairchild, I.J., 2001. Partitioning of Sr^{2+} and Mg^{2+} into calcite under karst-analogue experimental conditions. Geochim. Cosmochim. Acta 65, 47–62.

Ihlenfeld, C., Norman, M.D., Gagan, M.K., Drysdale, R.N., Maas, R., Webb, J., 2003. Climatic significance of seasonal trace element and stable isotope variations in a modern freshwater tufa. Geochim. Cosmochim. Acta 67, 2341–2357.

Ivany, L.C., Runnegar, B., 2010. Early Permian seasonality from bivalve $\delta^{18}O$ and implications for the oxygen isotopic composition of seawater. Geology 38, 1027–1030.

Jennings, D.S., Lovelace, D.M., Driese, S.G., 2011. Differentiating paleowetland subenvironments using a multi-disciplinary approach: an example from the Morrison Formation, South Central Wyoming, USA. Sediment. Geol. 238, 23–47.

Jurkiewicz-Karnkowska, E., 2005. Some aspects of nitrogen, carbon and calcium accumulation in molluscs from the Zegrzyński reservoir ecosystem. Pol. J. Environ. Stud. 14, 173–177.

Kontrec, J., Kralj, D., Brecevic, L., Falini, G., Fermani, S., Noethig-Laslo, V., Mirosavljevic, K., 2004. Incorporation of inorganic anions in calcite. Eur. J. Inorg. Chem. 23, 4579–4585.

Leinfelder, R.R., Hartkopf-Fröder, C., 1990. In situ accretion mechanism of concavo-convex lacustrine oncoids ("swallow nests") from the Oligocene of the Mainz Basin, Rhineland, FRG. Sedimentology 37, 287–301.

Lepvrier, C., Martínez García, E., 1990. Fault development and stress evolution of the post-Hercynian Asturian Basin (Asturias and Cantabria, northwestern Spain). Tectonophysics 184, 345–356.

Lindqvist, J.K., 1994. Lacustrine stromatolites and oncoids: Manuherikia Group (Miocene), New Zealand. 1. In: Bertrand-Sarfati, C. Monty (Ed.), Phanerozoic Stromatolites II, pp. 227–254.

Lorens, R.B., 1981. Sr, Cd, Mn and Co distribution coefficients in calcite as a function of calcite precipitation rate. Geochim. Cosmochim. Acta 45, 553–561.

McKirdy, D.M., 1976. Biochemical markers in stromatolites. In: Walter, M.R. (Ed.), Stromatolites. Dev. Sedimentol 20, pp. 163–191.

McKirdy, D.M., Hayball, A.J., Warren, J.K., Edwards, D., von der Borch, C.C., 2010. Organic facies of Holocene carbonates in North Stromatolite Lake, Coorong region, South Australia. Cad. Lab. Xeol. Laxe. 35, 127–146.

Meléndez, G., García-Ramos, J.C., Valenzuela, M., Suárez de Centi, C., Aurell, M., 2002. Jurassic. Asturias. In: Gibbons, W., Moreno, T. (Eds.), The Geology of Spain. Geol. Soc. London, pp. 213–215.

Morse, J.W., Wang, Q.W., Tsio, M.Y., 1997. Influences of temperature and Mg:Ca ratio on $CaCO_3$ precipitates from seawater. Geology 25, 85–87.

Mucci, A., 1988. Manganese uptake during calcite precipitation from seawater: conditions leading to the formation of a pseudokutnahorite. Geochim. Cosmochim. Acta 52, 1859–1868.

Mur, L.R., Skulberg, O.M., Utkilen, H., 1999. Cyanobacteria in the environment (Chapter 2) In: Chorus, I., Bartram, J. (Eds.), Toxic Cyanobacteria in Water: A Guide to their Public Health Consequences, Monitoring and Management. E & FN Spon, New York, pp. 15–40.

Naeher, S., Gilli, A., North, R.P., Hamann, Y., Schubert, C.J., 2013. Tracing bottom water oxygenation with sedimentary Mn/Fe ratios in Lake Zurich, Switzerland. Chem. Geol. 352, 125–133.

Neuhauser, K.R., Lucas, S.G., De Albuquerque, J.S., Louden, R.J., Hayden, S.N., Kietzke, K.K., Oakes, W., Des Marais, D., 1987. Stromatolites of the Morrison formation (Upper Jurassic), Union County, New Mexico. A Preliminary Report: New Mexico Geological Society Guidebook, 38th Field Conference, Northeastern New Mexico, pp. 153–159.

Ordóñez, S., González Martín, J.A., García del Cura, M.A., Pedley, H.M., 2005. Temperate and semi-arid tufas in Pleistocene to Recent fluvial barrage system in the Mediterranean area: the Ruidera Lakes Natural Park (Central Spain). Geomorphology 69, 332–350.

Pavlovic, G., Prohic, E., Miko, S., Tibljas, D., 2002. Geochemical and petrographic evidence of meteoric diagenesis in tufa deposits in Northern Dalmatia (Zrmanja and Krupa Rivers, Croatia). Facies 46, 27–34.

Pentecost, A., 2005. Travertine. Springer, Berlin (445 pp.).

Perry, C.T., 1994. Freshwater tufa stromatolites in the basal Purbeck Formation (Upper Jurassic), Isle of Portland, Dorset. Geol. J. 29, 119–135.

Pirrie, D., Marshall, J.D., 1990. Diagenesis of Inoceramus and Late Cretaceous paleoenvironmental geochemistry: a case study from James Ross Island. Antarct. Palaios 5, 336–345.

Purton, L., Shields, G.A., Brasier, M.D., Grime, G.W., 1999. Metabolism controls Sr/Ca ratios in fossil aragonitic mollusks. Geology 27, 1083–1086.

Qvarnström, M., 2012. An Interpretation of Oncoid Mass-occurrence During the Late Silurian Lau Event, Gotland, Sweden. Thesis of Department of Geology, Lund University (20 pp.).

Ramírez del Pozo, J., 1969. Bioestratigrafía y paleogeografía del Jurásico de la costa asturiana (zona de Oviedo-Gijón-Villaviciosa). Bol. Geol. Min. 80, 307–332.

Robles, S., Quesada, S., Rosales, I., Aurell, M., Meléndez, G., Bádenas, B., 2002. Jurassic Basque-Cantabrian Basin. In: Gibbons, W., Moreno, T. (Eds.), The Geology of Spain. Geol. Soc. London, pp. 215–221.

Rossi, C., Mertz-Kraus, R., Osete, M.L., 2014. Paleoclimate variability during the Blake geomagnetic excursion (MIS 5d) deduced from a speleothem record. Quat. Sci. Rev. 102, 166–180.

Sandberg, P.A., Hudson, J.D., 1983. Aragonite relic preservation in Jurassic calcite-replaced bivalves. Sedimentology 30, 879–892.

Sandford, R.F., 1995. Hydrogeology of Jurassic and Triassic wetlands in the Colorado Plateau and the origin of the tabular sandstone uranium deposits. U.S. Geol. Surv. Prof. Pap. 1548, 1–40.

Schudack, U., 1987. Charophytenflora und fazielle Entwicklung der Grenzschichten mariner Jura/Wealden in den Nordwestlichen Iberischen Ketten (mit Vergleichen zu Asturien und Kantabrien). Palaeontogr. Abt. B 204, 1–180.

Schudack, U., Schudack, M., 2002. New biostratigraphical data for the Upper Jurassic of Asturias (northern Spain) based on Ostracoda. Rev. Esp. Micropaleontol. 31, 1–18.

Słowakiewicz, M., Tucker, M.E., Pancost, R.D., Perri, E., Mawson, M., 2013. Upper Permian (Zechstein) microbialites: supratidal through deep subtidal deposition, source rock, and reservoir potential. AAPG Bull. 97, 1921–1936.

Staudt, W.J., Schoonen, M.A.A., 1995. Sulfate incorporation into sedimentary carbonates. In: Vairavamurthy, M.A., Schoonen, M.A.A. (Eds.), Geochemical Transformations of Sedimentary Sulfur. American Chemical Society, Washington, D.C, pp. 332–345.

Szulc, J., Gradziński, M., Lewandowska, A., Heunisch, C., 2006. The Upper Triassic crenogenic limestones in Upper Silesia (southern Poland) and their paleoenvironmental context. In: Alonso-Zarza, A.M., Tanner, L.H. (Eds.), Paleoenvironmental Record and Applications of Calcretes and Palustrine Carbonates. Geol. Soc. Am., Spec. Pap. 416, pp. 133–151.

Takano, B., Asano, Y., Watanuki, K., 1980. Characterization of sulfate ion in travertine. Contrib. Mineral. Petrol. 72, 197–203.

Talbot, M.R., 1990. A review of the paleohydrological interpretation of carbon and oxygen isotopic ratios in primary lacustrine carbonates. Chem. Geol. 80, 261–279 (Isotope Geoscience Section).

Tooth, S., McCarthy, T.S., 2007. Wetlands in drylands: geomorphological and sedimentological characteristics, with emphasis on examples from southern Africa. Prog. Phys. Geogr. 31, 3–41.

Treese, T.N., Owen, R.M., Wilkinson, B.H., 1981. Sr/Ca and Mg/Ca ratios in polygenetic carbonate allochems from a Michigan marl lake. Geochim. Cosmochim. Acta 45, 439–445.

Uzkeda, H., Bulnes, M., Poblet, J., García-Ramos, J.C., Piñuela, L., 2013. Buttressing and reverse reactivation of a normal fault in the Jurassic rocks of the Asturian Basin, NW Iberian Peninsula. Tectonophysics 599, 117–134.

Valenzuela, M., García-Ramos, J.C., Suárez de Centi, C., 1986. The Jurassic sedimentation in Asturias (N Spain). Trab. Geol. Univ. Oviedo 16, 121–132.

Webb, G.E., Price, G.J., Nothdurft, L.D., Deer, L., Rintoul, L., 2007. Cryptic meteoric diagenesis in freshwater bivalves: implications for radiocarbon dating. Geology 35, 803–806.

Weiner, S., Dove, P.M., 2003. An overview of biomineralization and the problem of the vital effect. In: Dove, P.M., Weiner, S., De Yoreo, J.J. (Eds.), BiomineralizationRev. Mineral. Geochem. 54. Mineralogical Society of America, pp. 1–31.

Whiteside, J.H., 2005. Hierarchy of carbon cycle modulation in cyclical Late Triassic–Early Jurassic age lacustrine strata, Newark Supergroup, USA. Abstracts for International Symposium on the Jurassic Boundary EventsThe First Symposium of IGCP 506 (Nov. 1–4, Nanjing, China.).

Wright, V.P., Cherns, L., 2009. Selective dissolution of aragonite during shallow burial and the implications for carbonate sedimentology. In: Lukasik, J., Simo, J.A. (Eds.), Controls on Carbonate Platform and Reef Development: Tulsa. SEPM Spec. Pub 89, pp. 47–54.

Yan, H., Lee, X., Zhou, H., Cheng, H., Peng, Y., Zhou, Z., 2009. Stable isotope composition of the modern freshwater bivalve *Corbicula fluminea*. Geochem. J. 43, 379–387.

Yan, H., Chen, J., Xiao, J., 2014. A review on bivalve shell, a tool for reconstruction of paleoclimate and paleo-environment. Chin. J. Geochem. 33, 310–315.

Zamarreño, I., Anadón, P., Utrilla, R., 1997. Sedimentology and isotopic composition of Upper Palaeocene to Eocene non-marine stromatolites, eastern Ebro Basin, NE Spain. Sedimentology 44, 159–176.

Zaton, M., Kremer, B., Maryknowski, L., Wilson, M.A., Krawczynski, W., 2012. Middle Jurassic (Bathonian) encrusted oncoids from the Polish Jura, southern Poland. Facies 58, 57–77.

Ziegler, P.A., 1990. Geological Atlas of Western and Central Europe. Shell Intern. Petrol. Maats. B.V 2nd ed. 2. The Hague.